CZECH TECHNICAL UNIVERSITY IN PRAGUE
FACULTY OF MECHANICAL ENGINEERING
DEPARTMENT OF ENVIRONMENTAL ENGINEERING

NOISE GENERATED BY AIR DISCHARGED FROM SMALL OPENINGS

BACHELOR'S THESIS

HASSAN AHMED ZAKARIA
HASSAN AMIN

1 – EE – 2020

Summary

In this experimental thesis, aerodynamic noise generated by holes of different diameters in a duct system is evaluated. In the first part of the thesis can be found a small introduction to noise and the effects it has on modern-day citizens. Then aerodynamic noise caused in HVAC systems is briefly introduced. The second and main part of the thesis is the experimental part. The evaluation of the mean airflow velocity over the leaks is the first part of the experiment and can be found in chapter (3) as well as list of equipment used, procedure, results and verification of the measurements, and the calculation of the tunnel constant. In chapter (4), the reader can find the procedure of measuring the aerodynamic noise as well the results of the relation between sound power level and third-octave band frequencies, Strouhal number and relative sound power levels, and finally the relation between total sound power level and the logarithm of velocity. Presented in the conclusion is a summary of the work and the most significant results found as well as some suggestions for improving the measurements in the future.

Acknowledgment

I would like to extend my deepest thanks to my supervisor Ing. Miroslav Kučera Ph.D. for his intellectual guidance through the course of my work, and to Ing. Jan Králíček for his tremendous help with the measurements and the evaluation of the data. And to my family and friends for their unconditional love and support throughout the course of my studies.

Hassan Amin.

Declaration

I declare that this diploma thesis entitled "Noise generated by air discharged from small holes" is my own work performed under the supervision of Ing. Miroslav Kučera Ph.D., with the use of the literature presented at the end of my diploma thesis in the list of references.

In Prague 06.01.2020 ----------

Hassan Amin

Table of Contents

List Of Used Symbols

Symbol	Unit	Meaning
Xi	[-]	tunnel constant
P_d	[Pa]	dynamic pressure
P_s	[Pa]	static overpressure
ρ	[kg/m^3]	density of air
v_s	[m/s]	average velocity of air 3 mm above the leaks
p_b	[Pa]	barometric pressure
p_v	[kg/m^3]	saturated vapor pressure
r_a	[J/Kg/K]	specific gas constant of dry air
t_d	[℃]	dry bulb temperature
L_w	[dB]	sound power level
L_p	[dB]	sound pressure level
S	[m^2]	area of half sphere
L'_p	[dB]	average sound pressure level
N	[-]	number of points
L_i	[dB]	sound pressure level
L_p	[dB]	Corrected sound pressure level,
L_p	[dB]	Sound pressure level for a given third octave band,
$L_{p,background}$	[dB]	background noise level for a given third octave band.
S	[-]	Strouhal number
f	[Hz]	third-octave band frequency
d	[m]	diameter of the leaks
$L_{w,rel}$	[dB]	relative sound power level
L_w	[dB]	total sound power level
$L_{w,i}$	[dB]	spectrum of the sound power level

L_{wA}	[dB]	sound power level corrected by filter A
K_{Ai}	[dB]	weighted filter A

Part 1: Theoretical Part:

1. Introduction:

In modern-day society, where productivity and comfort are increasingly becoming a prerequisite for success in most businesses and industries, and where lack of proper acoustic treatment in buildings can interfere with the efficient functioning of people, noise is one of the main issues to be dealt with in order to achieve high standards of comfort and, subsequently, success.

Sound travels through a medium in a series of compressions and rarefactions, causing disturbances in the medium through which it travels, and that we hear as sound. A sound wave in its simplest form is sinusoidal in nature with a wavelength and frequency[1]. The range of audible frequencies is generally known to be between 20 Hz and 20 kHz, and the frequencies falling outside this range are said to be imperceptible, although this range can vary between one person and the other.

Sound is a vital part of our lives. It's how we communicate with one another and how we express our emotions. Many sounds are popularly recognized as enjoyable sounds like the sound of music, many others, however, like microphone feedback, are known as noise.

Noise is generally labeled as an unwelcome or undesired sound, and it affects people differently. When a person is exposed to noise above a certain level, there is a real danger of partial, if not permanent hearing loss. The threshold of hearing is frequency-dependent but it's generally known at 1000 Hz to be at 0 dB and the threshold of pain at 140 dB[2]. That's why noise control is an essential practice in reducing the risk associated with high and continuous levels of noise exposure.

Flow-generated noise in the indoors, however, like that generated in HVAC systems, is more associated with discomfort than danger to health. There have only been a few studies that tried to tackle that problem and most research is focused on the field of aviation.

Much of the early work and the progress made thus far in the field of aeroacoustics can be credited to Sir Michael James Lighthill who is considered a pioneer in aeroacoustics. Lighthill's analogy, established in 1952, made a connection between fluid mechanics and acoustics by rearranging the Navier-Stokes equations, which describe the motion of a viscous fluid, into a wave equation.[3]

My focus in this experimental thesis is aerodynamic noise, which is the noise generated by the flow of air, but not just any flow, the flow needs to be turbulent, i.e, above a certain value of dimensionless Reynolds number(ratio between inertial forces and viscous forces). The science of aeroacoustic started when the need for understanding the behavior of the jet engine for commercial aircraft and the development of the science of Aviation in the 1950s[4], which makes it quite a brand new field of science. The aim was to make the noise generated from jet aircraft more acceptable for people living near airports, who, before the invention of commercial flights, were living a more tranquil life. Aerodynamic noise is a rather complicated topic due to the fact that it deals with turbulent flows whose behavior is chaotic, random and hard to predict. This research is but an attempt to better understand it and expand the knowledge that has been around for only a few decades. Not enough experiments have been done to try to understand aerodynamic noise generated at low velocities/low Mach numbers through small holes, and this experiment is part of the ongoing effort to form a better view on it.

First off, I will start by briefly introducing the sources of flow generated noise in HVAC systems, then I will proceed into the main part which is the experimental one.

2. Aerodynamic Noise:

2.1. Sources of Aerodynamic Noise:

2.1.1 HVAC systems:

The main aim of HVAC (Heating, Ventilation & Air Conditioning) systems is to provide thermal comfort as well as good air quality to the areas through which they operate. Both air and water/steam systems exist, but the main focus here will be about air distribution systems. Noise in HVAC systems is usually the byproduct of both mechanical equipment(fans, pumps, refrigeration equipment) and flow-generated noise(aerodynamic noise). Flow-induced noise, even though sometimes less perceptible than mechanical, can usually be a source of irritation and annoyance for the people in the rooms, mainly at the terminal end of the HVAC systems. Air flowing from the fan to the diffuser passes through ducts. Noise is generated in every step of the way, starting from the fan, passing by the ducts, whether it's straight or obstructed by some bends or elbows, terminating at the diffuser which is an impediment to airflow.

2.1.1.1 Straight Duct noise:

As discussed earlier, aerodynamic noise is a type of self-induced noise, and that's exactly the case when air is flowing through a straight uninterrupted duct. This noise is generated by fluctuations in pressure caused by the unsteady, turbulent flow of air, which, in turn, could generate structural vibrations causing more noise. Eddies in the flow generate noise when they bump into irregularities in the pipe cross-section causing the flow to accelerate and decelerate[5], thus, to control the duct velocity, the cross-sectional area must be either increased or decreased depending on the desired outcome of the system. Flow noise in straight ducts is not particularly noisy when compared with other duct generated sounds.

2.1.1.2 Transition Duct Noise:

When air flowing through a duct encounters a change in the cross-sectional area, whether it's a sudden or gradual transition, significant aerodynamic noise is generated. If air is flowing with a high velocity and the transition is sudden, as in the case of a leak, higher turbulence occurs and the aerodynamic noise generated is louder than in the case of slower flow velocities and gradual alteration.[5] However, slower velocities can generate tonal components when passing through a small abrupt change in area, which will be shown more broadly in the experimental part of the thesis.

2.1.1.3 Diffuser Generated Noise:

Diffusers/Grills are the terminal ends of most air distribution systems and the ones most vulnerable to noise emissions[6], either through the vibration of the diffuser blade, or the aerodynamic noise caused by the turbulent flow of air due to the obstruction of the diffuser blade to the airflow. Diffuser noise is influenced by air velocity through the system. Unlike noise generated by the ventilator in HVAC systems which can be dampened, reducing noise generated by air velocity at the diffuser can be achieved by either increasing the size or number of diffusers.

In the next part of the thesis, aerodynamic noise generated by leaks in an HVAC system will be studied. Leaks in an HVAC system are a serious source of noise and sometimes they're hard to identify. Noise generated by air flowing at low velocities through small leaks is often accompanied by a whistling sound due to the diffusion of air from a small area to a bigger one which can be very irritating to the listener. This whistling sound was observed in the measurements of aerodynamic noise that will be shown in chapter (4). The leaks studied are characterized by very small diameters and bigger length and their behavior will be shown graphically.

Part 2: Experimental Part

The aim of this experimental thesis is to measure and evaluate the aerodynamic noise generated by small holes from ducts. As well as to measure the flow velocity and the static gauge pressures in the duct.

The experiments were conducted in the acoustics laboratory on the ground floor of block G3 in the Faculty of Mechanical Engineering at the Czech Technical University in Prague. In the adjacent workshop room, is a ventilator fan that's responsible for inducing airflow through the duct system which leads to the acoustic laboratory. The terminal part of the duct system opens up to a nozzle that is fitted with a metal sheet for supporting the plexiglass/iron plates that are used for controlling the diameter of the leaks.

3. Quality of the Flowfield

In this chapter, the foundations for the aerodynamic noise measurements are laid. The velocity of the air supplied by the ventilator fan is measured 3 millimeters above the edge and in the middle of the leaks diameter, and the mean airflow velocity is determined. All data were exported to an MS excel program which was created for easier calculations of such measurements. The mean air velocity is then used to determine the tunnel constant which is essential in aerodynamic noise measurements for adjusting the desired airflow from the nozzle based on the static overpressure in the nozzle.

3.1 Equipment Used:

The following equipment was used in the measurement procedure:

1- The ventilation fan: The fan, located in the workshop room adjacent to the acoustics laboratory, is responsible for generating the air flowing through the duct system. It is fitted with a frequency attenuator for adjusting the fan speed. In this experiment, the initial frequency of the fan was set to be 10Hz then increased to 20, 30, 40, and 50 Hz as the highest frequency that could be achieved by the fan.

2- The nozzle: The air flowing from the fan through the duct system terminates at the nozzle. The nozzle is mounted with a metal sheet of 5 mm width, and fitted over the metal sheet is a 2 mm gum to prevent any air leaks when the plexiglass/iron plates are fitted on the metal plate.

Figure 3-1 Nozzle with fitted metal plate and gum.

3- Hot-wire anemometer: A dantec hot-wire anemometer probe type 55 was used for measuring the airflow velocity above the leaks. The probe was set 3 mm above the end of the leaks and parallel to the axis of the leaks. The probe had to be approached with absolute care and efficiency to avoid causing any damage to it.

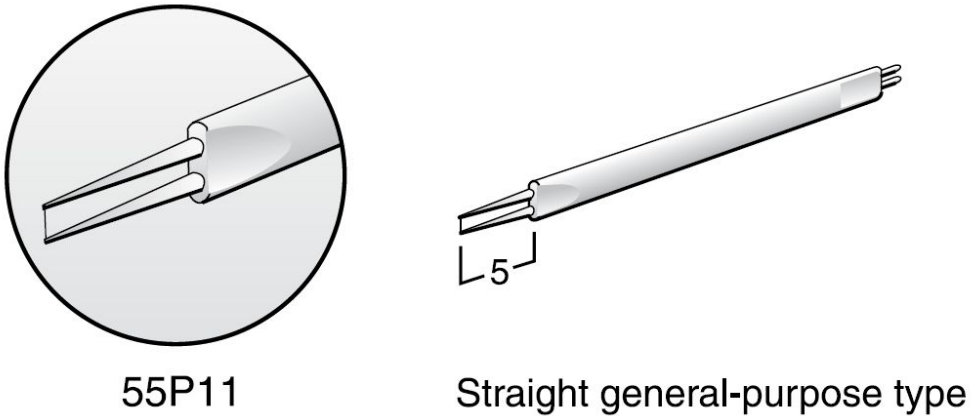

Figure 3-2 Dantec Hot-wire anemometer probe[9]

4- Probe Calibrator: Calibration of the probe was done each time before measuring the airflow velocity using dantec streamline 90H02 flow unit. The calibrator works by inducing some standard velocities and comparing them with the velocities measured by the hot-wire anemometer probe using a computer to which it was connected. In my case, 18 points were set between velocities 0,5 m/s and 60 m/s on a logarithmic scale, since the change in voltage is higher at lower velocities, with 8 iterations for each point. The sampling frequency was 10 kHz with 20,000 samples and recording time 2 seconds. The calibration graph is shown in Figure 3-6.

Figure 3-3 Dantec calibrator with dantec hot-wire anemometer probe mounted on it.

5- Traverse: The hot-wire anemometer probe was mounted on a traverse to control its movement in either x, y, or z axes over the surface of the leaks. The traverse was connected to a computer which was used to control its movement and the interval with which it moves.

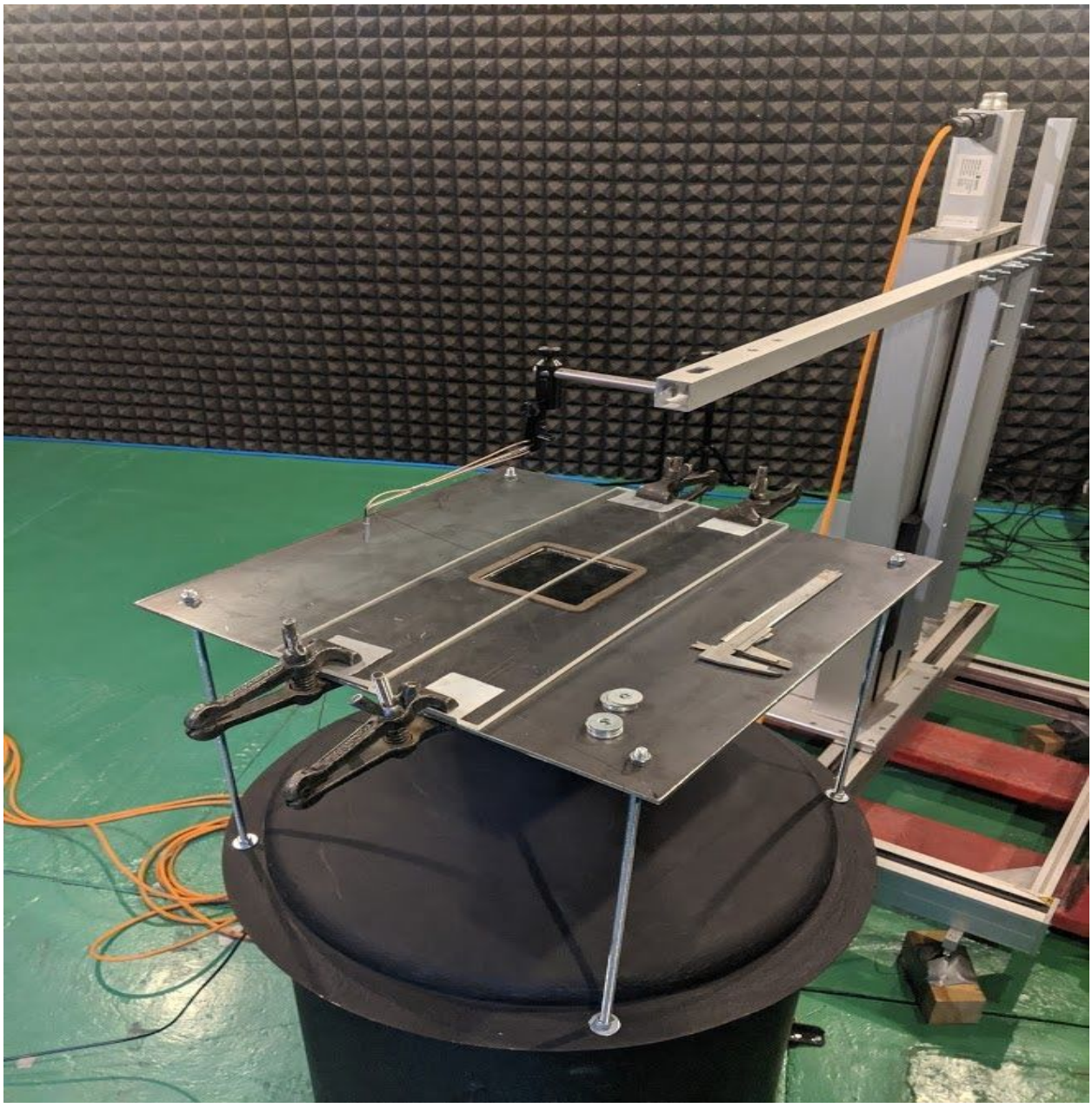

Figure 3-4 Hot-wire anemometer probe mounted on the traverse.

6- Plexiglass/iron plates: plexiglass and metal plates were used to constrict the flow from the nozzle and create the leakage for which the measurements were made. The plexiglass plate, shown in Figure 3-4 mounted on the metal sheet, has a thickness of 6 mm and the iron one has a thickness of 1 mm. The plates are clamped on the metal sheet by 4 clamps as seen in the figure above.

7- Rings: Also shown briefly in Figure 3-4 are metal rings with thickness 2,2 mm each. The rings were placed between the plastic/metal sheets to shape the size of the leakage then removed once the desired diameter was set. Initially, one ring was used to shape the leakage with diameter 2,2 mm. Secondly, 2 rings were placed for diameter 4,4 mm. Then 3 rings, then 4, until the final diameter reached was 11 mm using 5 rings.

8- Manometer: AIRFLOW MEDM 500 manometer was used to measure the static overpressure inside the nozzle when the frequency of the ventilator fan was changed. The manometer was connected to the nozzle using thin PVC tubes as shown in Figure 3-5.

Figure 3-5 AIRFLOW MEDM 500 manometer

The following figure is the wiring and connection diagram of all equipment used in the acoustics lab and the workshop in the adjacent room.

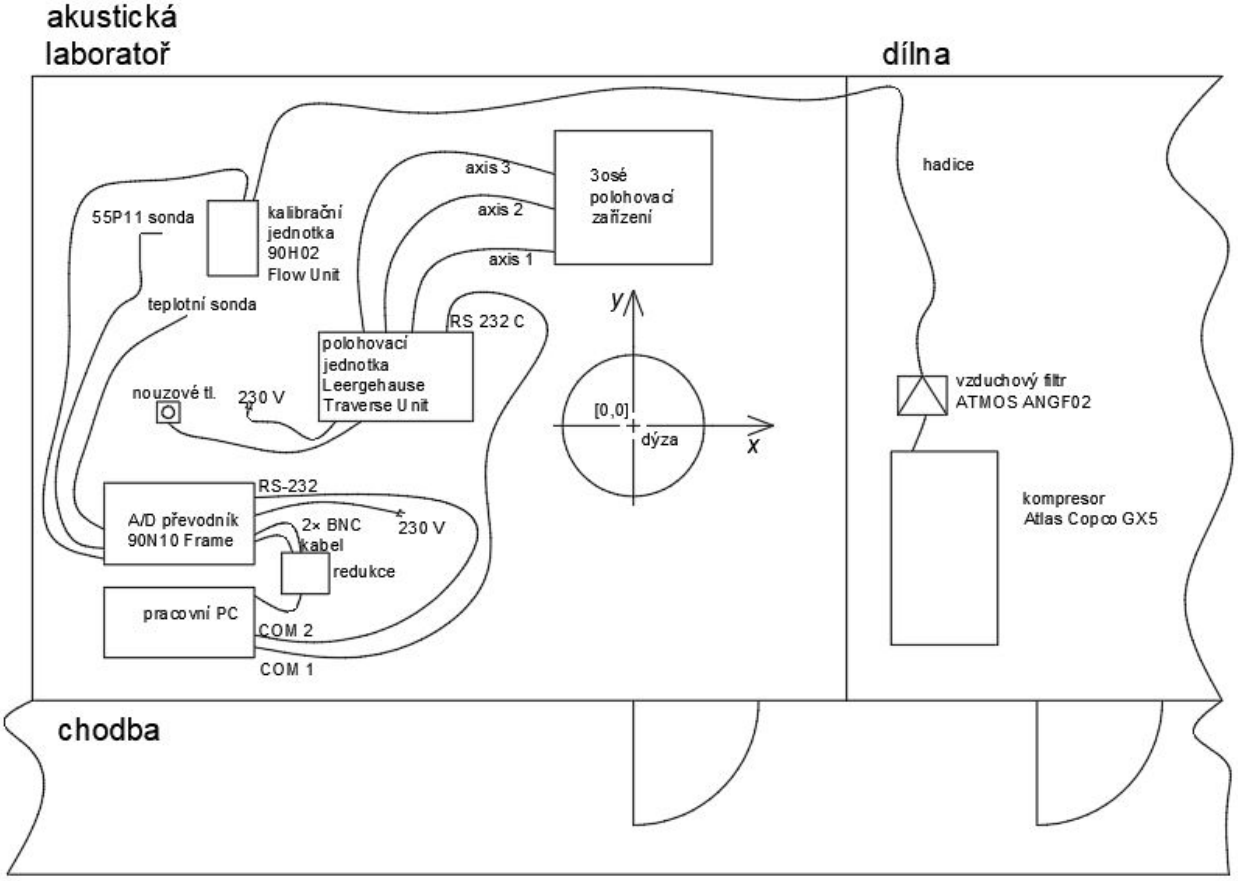

Figure 3-6 Connection diagram of the equipment used.[8]

3.1 Probe Calibration:

The airflow measurements were done over the course of three days, before each measurement, the probe had to be calibrated to make sure that the measurements would be as accurate as possible. As mentioned earlier, the calibration is done using dantec streamline 90H02 flow unit with the hot-wire anemometer probe mounted on it. The unit is connected to a computer that processes the data, which was then exported to an excel file for calculation and evaluation of the calibration graphs.

Calibration of the probe was performed by generating air with standard velocities through the calibration unit into the probe mounted on it, the probe registers the change in voltage and records the airflow velocity flowing through it and the computer records the data analyzed. The standard velocities set were at 18 points between velocities 0,5 m/s and 60 m/s with 8 iterations each with a sampling frequency of 10 kHz, 20,000 samples and recording time 2 seconds. The calibration graphs are presented as a function between the velocity measured and the voltage corrected by the probe.

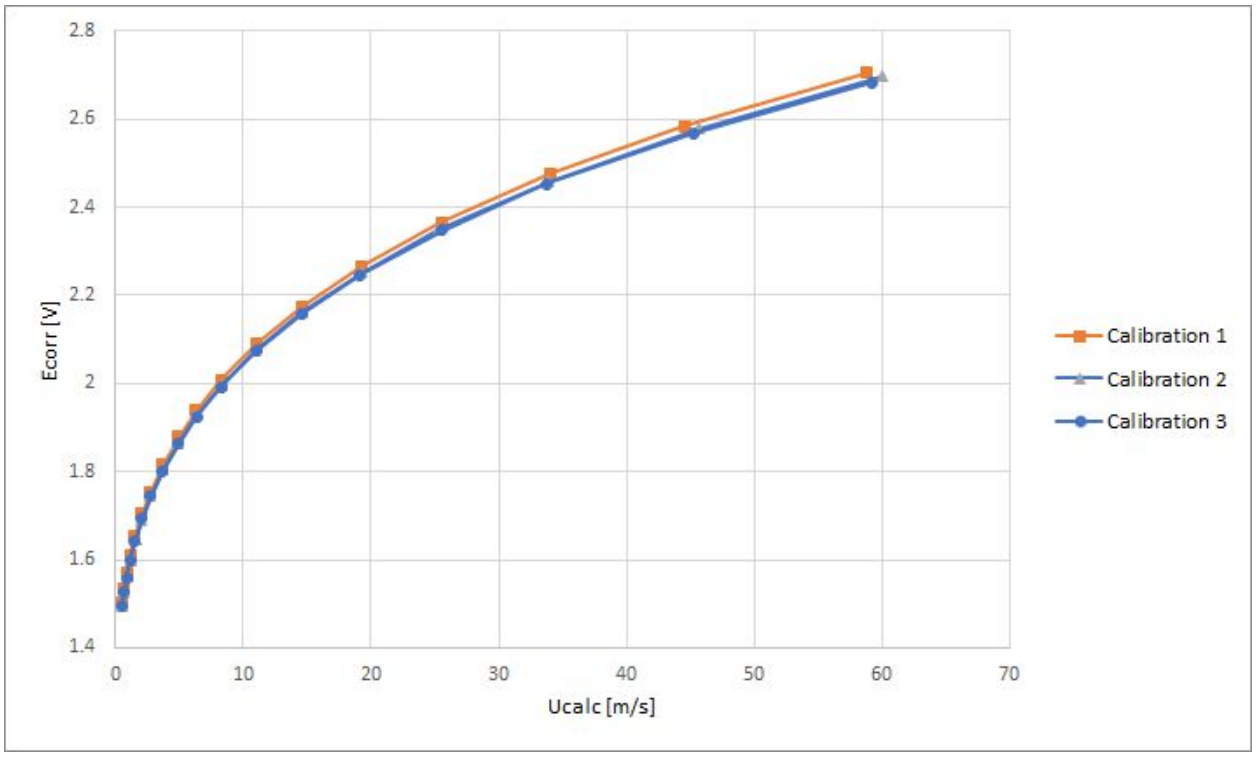

Figure 3-7 1st, 2nd, and 3rd Calibrations of the probe.

As can be seen in the graph, the three curves coincide together smoothly. Slight differences arise from the change in the conditions in the room(humidity, temperature, etc..) between one measurement and the next.

3.2 Measurements Procedure:

1- After the probe has been calibrated, it is then mounted on the traverse which is in turn connected to the computer that controls and directs its movements. The length of the leaks are 98 mm, but the traverse was set to start 13 mm before the leaks started and 13 mm after the leaks ended. The following figure shows the initial position of the probe over the nozzle:

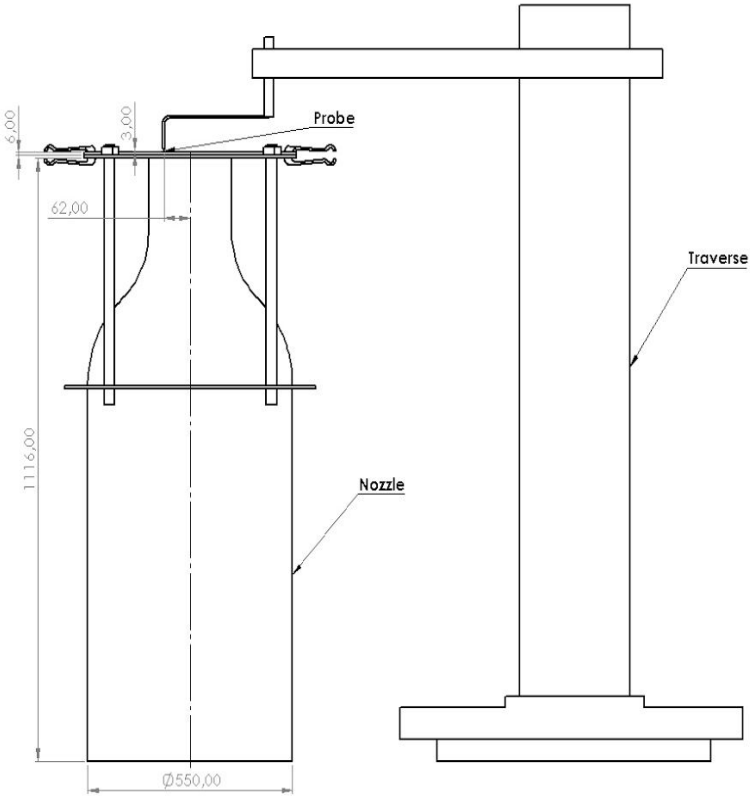

Figure 3-8 Initial position of the probe

2- Firstly, measurements were done for the plexiglass plate with 6 mm thickness . 2 sheets were used to constrict the flow of the air in the nozzle and separated by a metal ring with 2,2 mm thickness , which was then removed after the shape of the leaks was determined. Measurements were done for leaks with diameter 2,2/4,4/6,6/8,8 and 11 mm.

3- The ventilation fan in the adjacent room was then turned on. It had to be manually changed from 10 Hz to 20 Hz, 20 Hz to 30 Hz, and so on until 50 Hz was reached.

4- With the fan turned on, the probe in place(13 mm before the leaks began), and the shape of the leaks determined, the computer was then used to start the measurements.

3.3 Measurements Results:

1- Measurements were firstly done using the plexiglass plates to establish the leaks. The diameter of the leaks was set at 2,2 mm using one of the metal rings and frequency of the ventilator fan at 10 Hz, the traverse was set to travel along the length of the leaks with the probe set at a height of 3 mm above the end of the leaks as shown in Figure 3-8. With each step, the traverse stops, records the air velocity flowing through it, then moves 2 mm more, until the probe has traveled along the whole length of the leaks in addition to the 13 mm outside the leaks on each side.

2- The measurements recorded by the probe were processed by the computer and exported to an excel file for evaluation. The frequency of the fan was then increased to 20 Hz with the diameter of the leaks still at 2,2 mm. Once again the traverse travels along the whole length of the leaks, the measurements recorded by the probe, the computer processed the data and the excel file evaluates the values.

3- The measurements were repeated five times in total until the fan reached the maximum capacity of 50 Hz. The results are presented in the following graph:

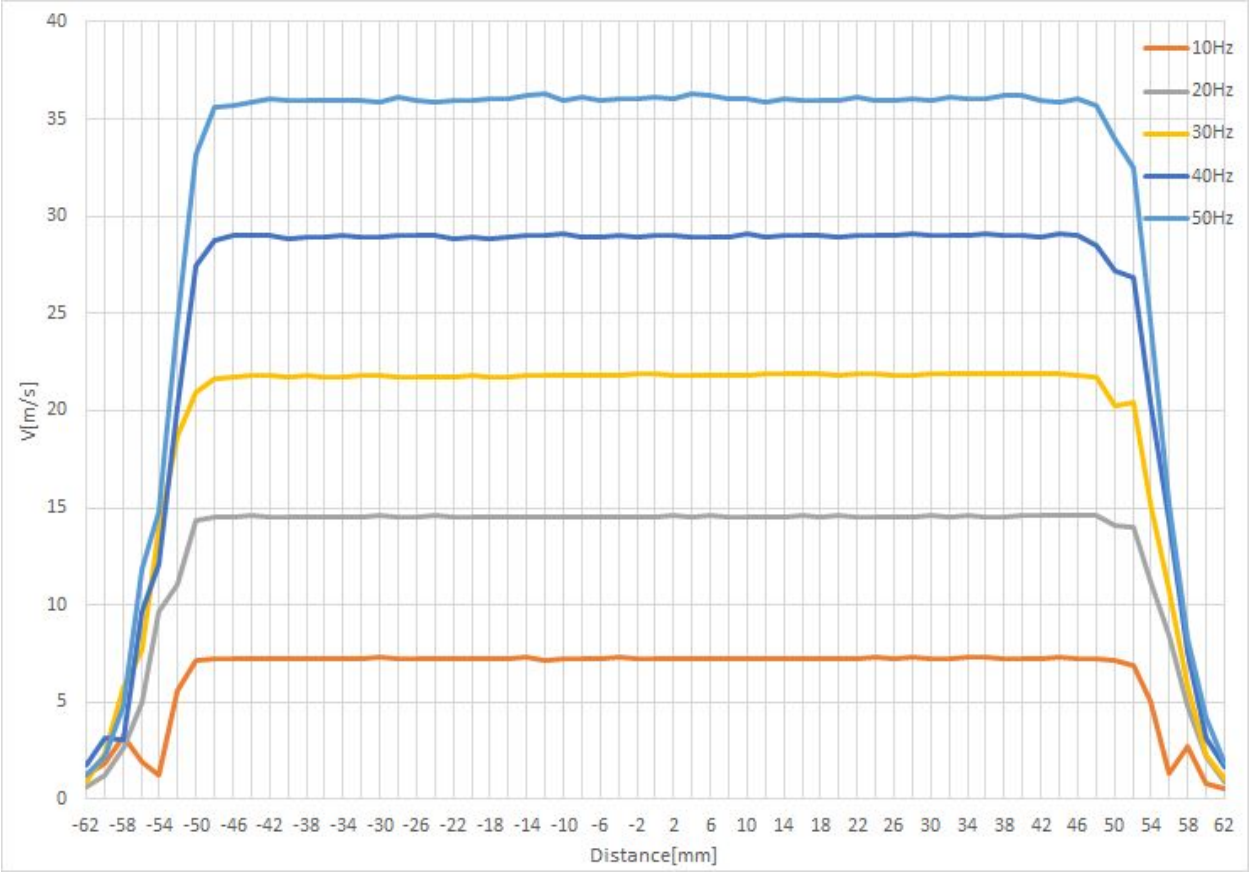

Figure 3-9 Velocity profile for diameter 2,2 mm across all fan frequencies.

In the previous diagram, it can be seen that the velocity of the airflow 3 mm above the leaks varies with the variation of the fan speed. The air velocity is almost zero before the leaks begin and just a few millimeters before the area of the leaks, the sudden rise in velocity happens and stays almost constant along the length of the leaks before dropping again after the leaks end. At 20 Hz, it can be seen that the airflow is not constant as in the other frequencies and this is not a standard situation. This could be either attributed to some error in the measurements or due to the big static overpressure in the nozzle caused by the leaks at this small diameter which will be more obvious in the aerodynamic noise measurements.

4- To increase the leakage diameter to 4,4 mm, 2 rings were now placed between the plexiglass plates and removed again once the diameter was shaped. The plexiglass plates were then clamped in position and the fan turned on at 10 Hz. The same procedure was followed as in the first diameter and the following results were obtained:

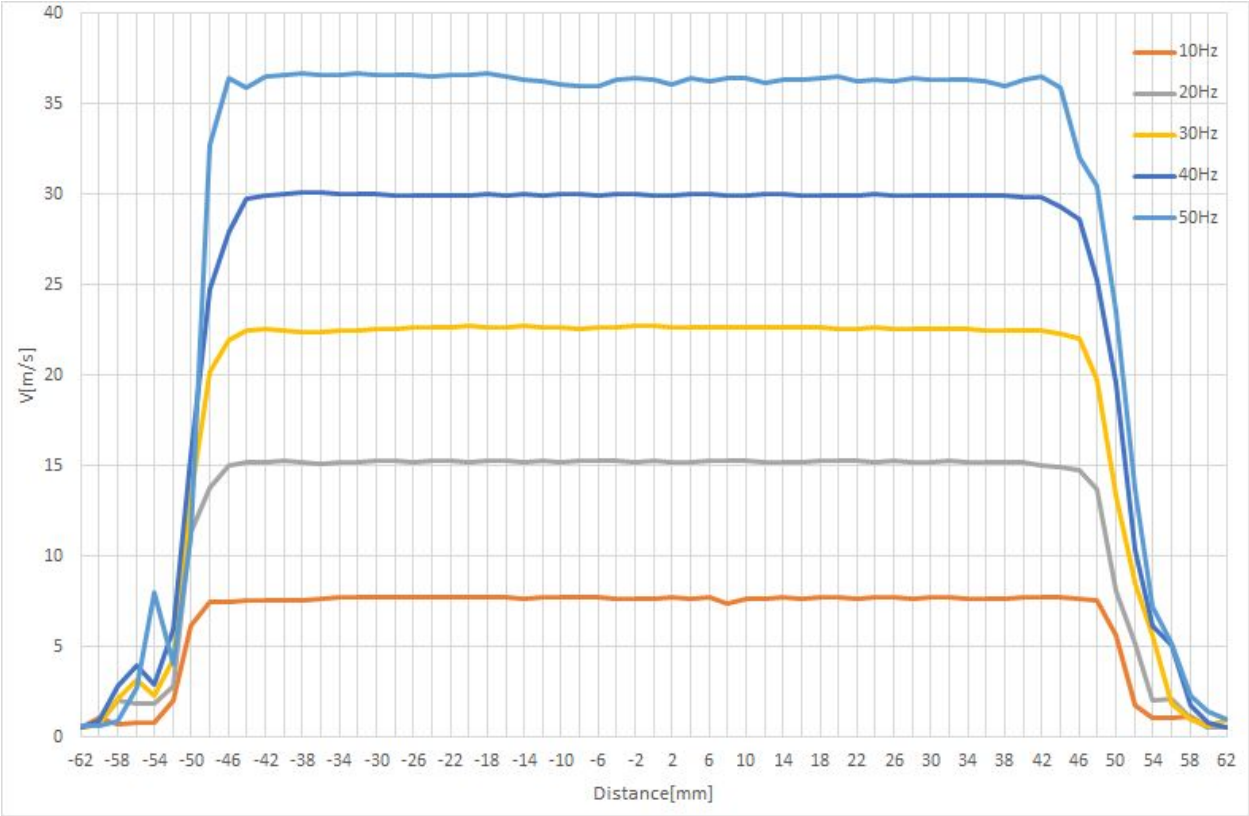

Figure 3-10 Velocity profile for diameter 4,4 mm across all fan frequencies.

5- The diameter was increased to 6,6/8,8 and 11 mm using the same method mentioned earlier and the results were obtained as follows:

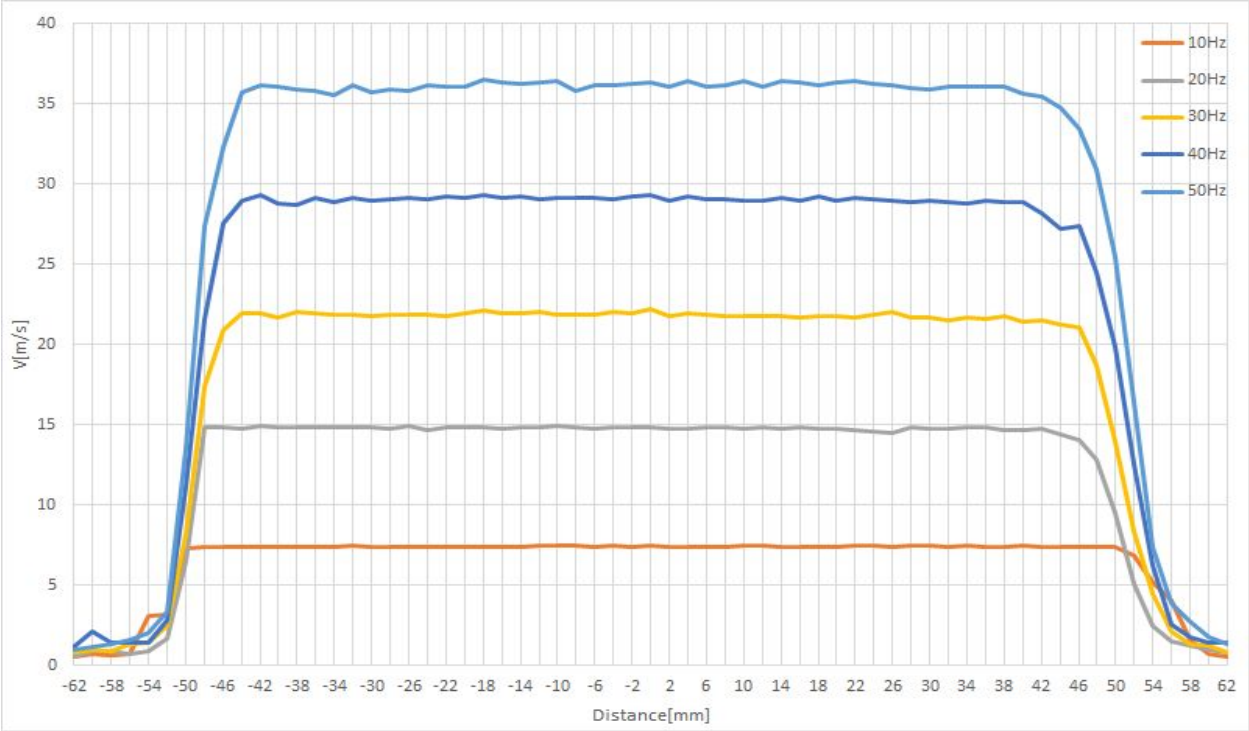

Figure 3-11 Velocity profile for diameter 6,6 mm across all fan frequencies.

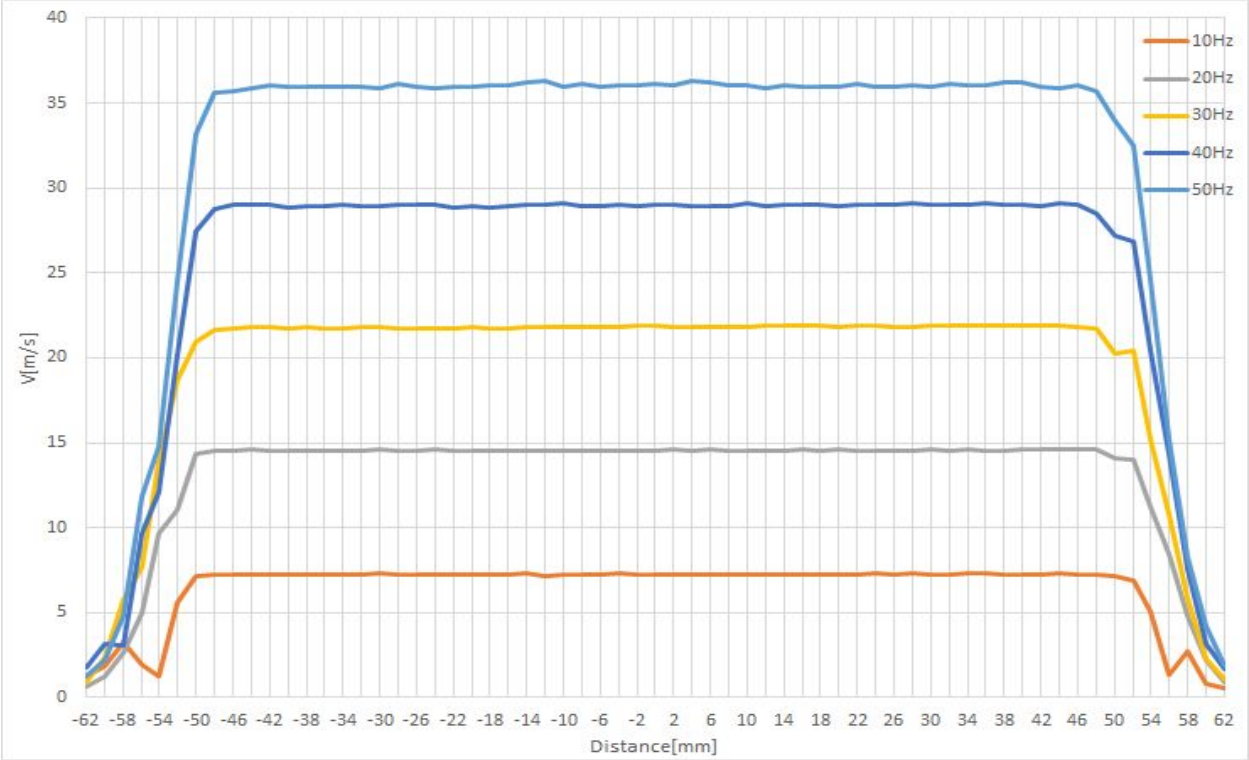

Figure 3-12 Velocity profile for diameter 8,8mm across all fan frequencies.

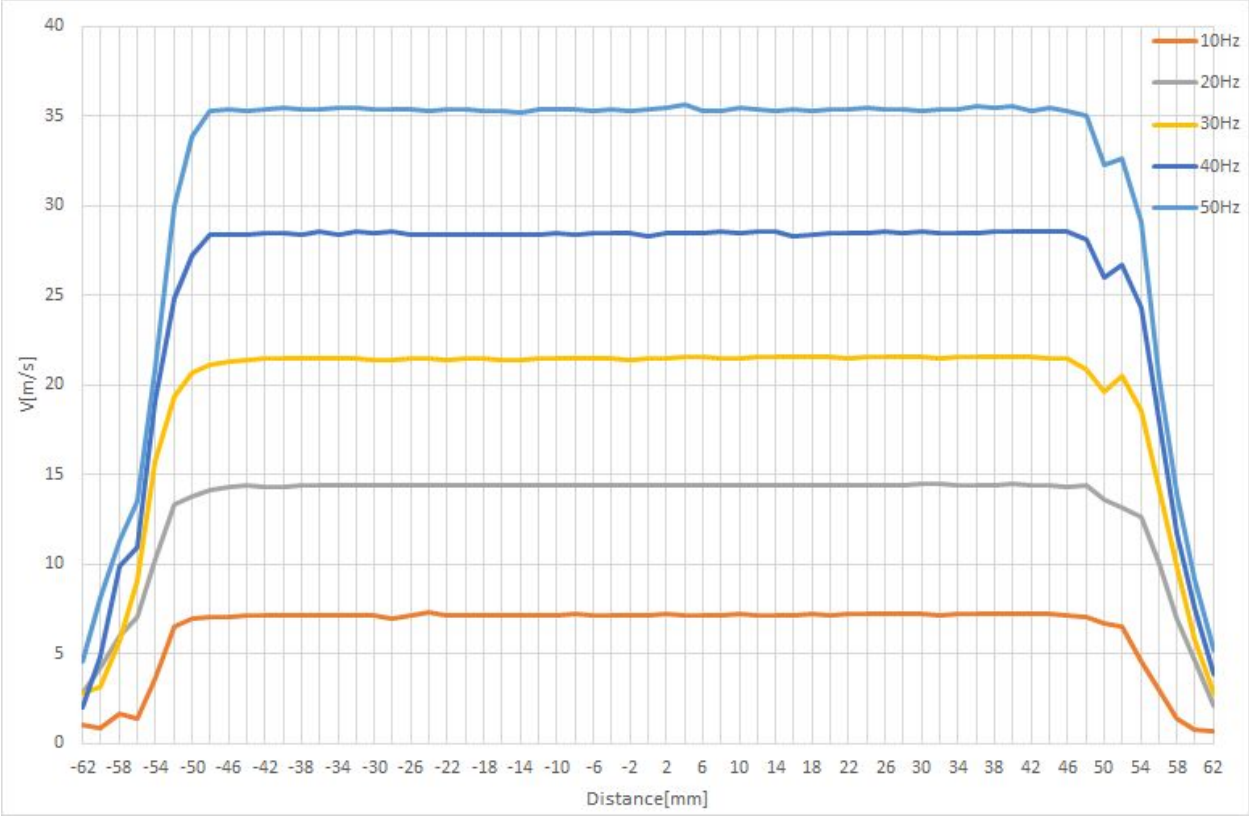

Figure 3-13 Velocity profile for diameter 11 mm across all fan frequencies.

From graphs 1, 2, 3, 4, and 5, it can be clearly seen that increasing the diameter of the leakage when the material used is plexiglass plate has little to no effect on the value of the mean airflow velocities along the leaks.

Measurements for the iron plate with thickness 1mm were done to just to verify whether changing the material used to constrict the leakage will change the static overpressure in the nozzle and the mean airflow velocity and eventually the aerodynamic noise. Hence, the iron plate measurements were done for the velocity of airflow with the fan ventilator at frequencies 30 and 50 Hz only. All measurement procedures were exactly the same as for the plexiglass plate. In the following graphs, I will present the combined graphs of both the plexiglass plate and the iron plate to verify how the changing of material and thickness of the plates might affect the airflow velocity and the shape of the flow field. The first graph shows the diagrams of the iron plate and plexiglass plate for 30 and 50 Hz frequency of the fan. The results are as follows:

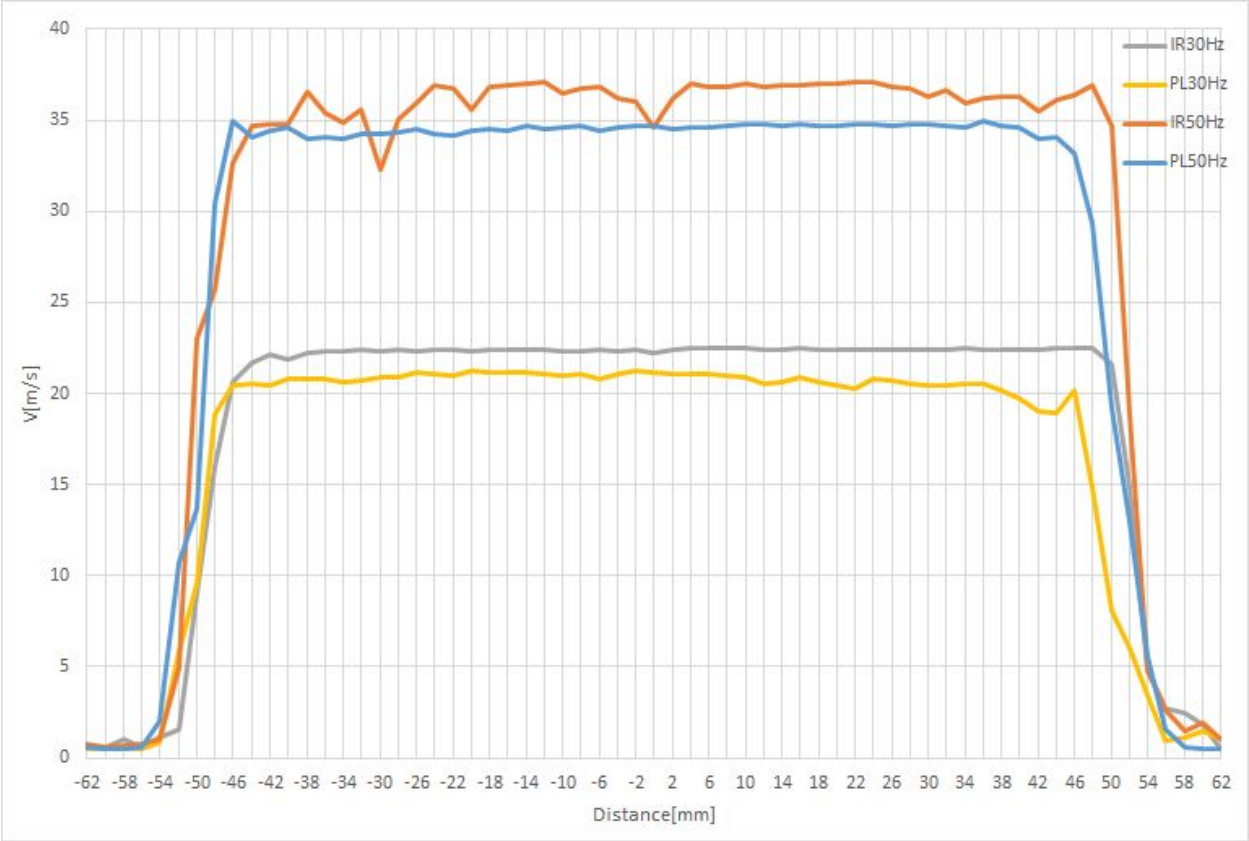

Figure 3-14 Velocity profile for Iron plate and plexiglass plate with diameter 2,2 mm and different frequencies of the fan.

It's shown in the previous diagram that for the same diameter of leaks and same fan velocity at 50 Hz, the iron plate diagram is way less constant. This is due to the higher intensity of turbulence caused by the thickness of the plate. This will be discussed further in the next chapter.

For the following graphs, the diameter was increased to 4,4/6,6/8,8 and 11 mm respectively and the results are as follows:

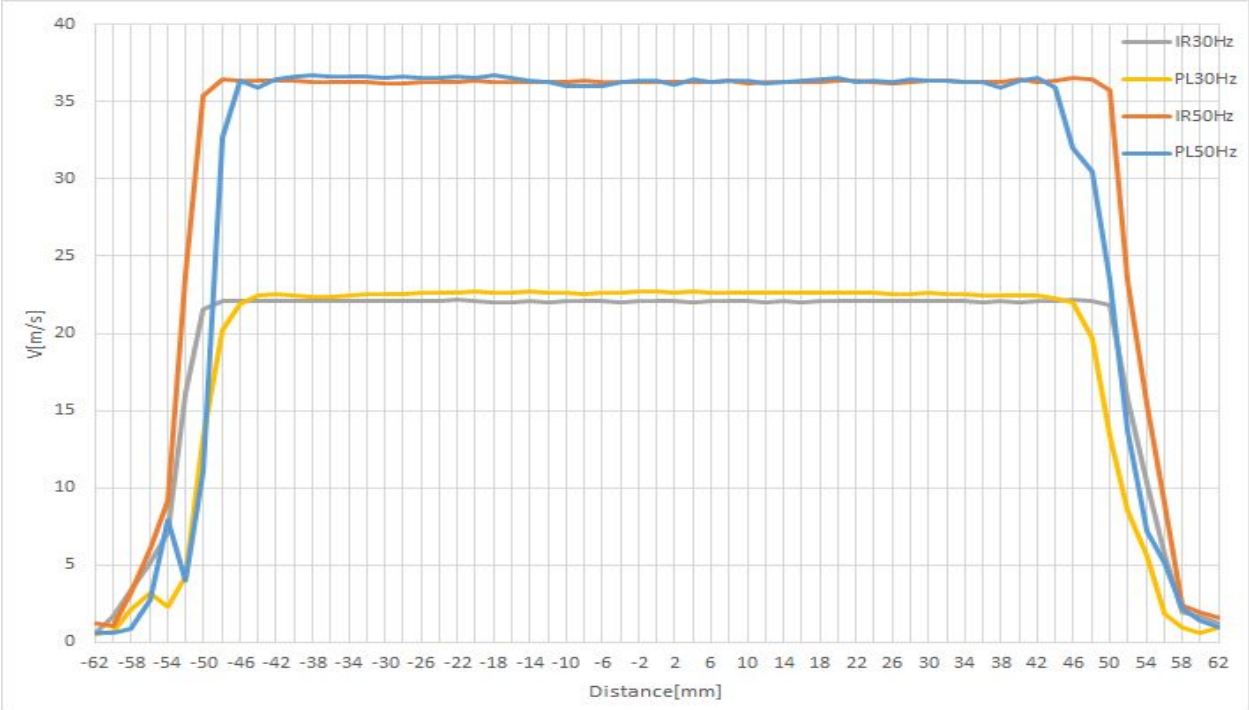

Figure 3-15 Velocity profile for Iron plate and plexiglass plate with diameter 4,4 mm and different frequencies of the fan.

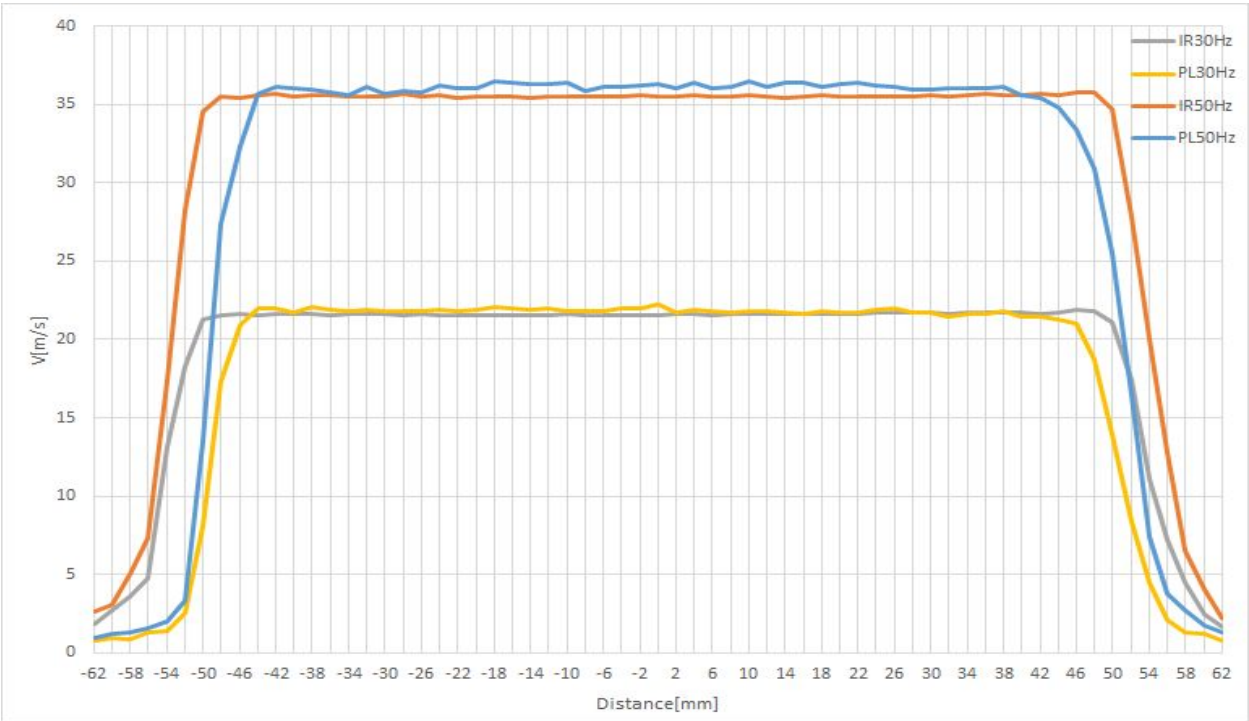

Figure 3-16 Velocity profile for Iron plate and plexiglass plate with diameter 6,6 mm and different frequencies of the fan.

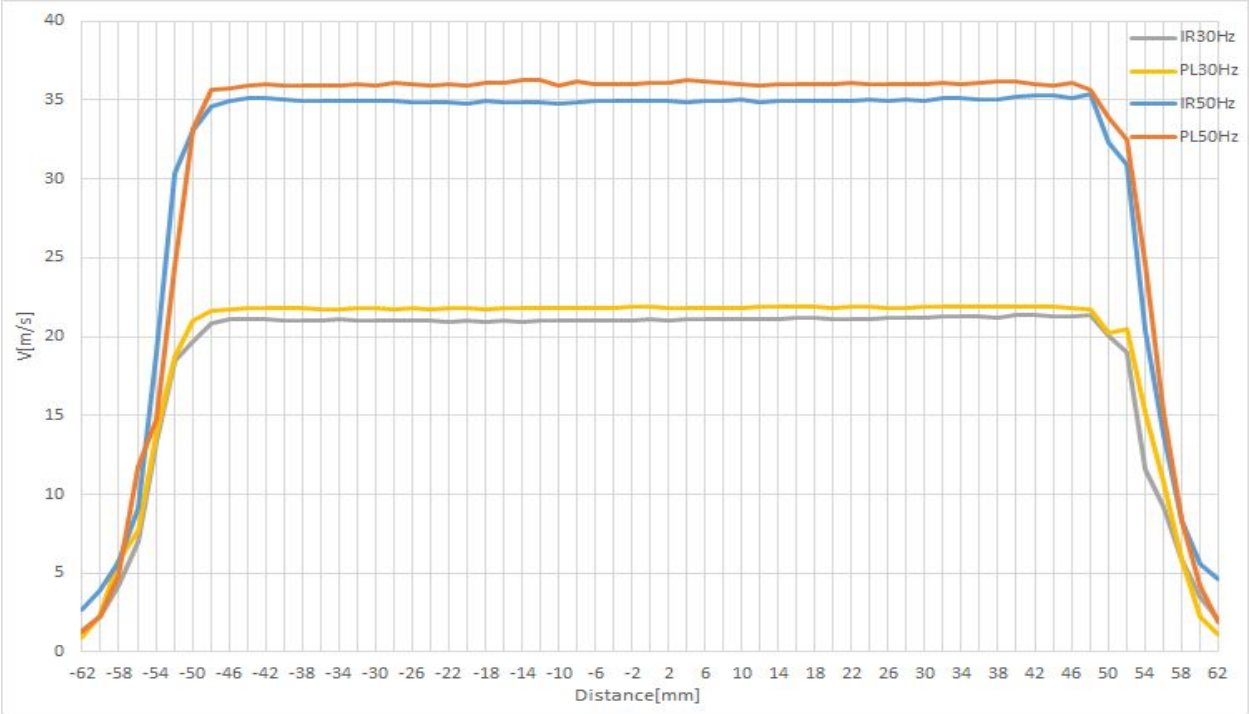

Figure 3-17 Velocity profile for Iron plate and plexiglass plate with diameter 8,8 mm and different frequencies of the fan..

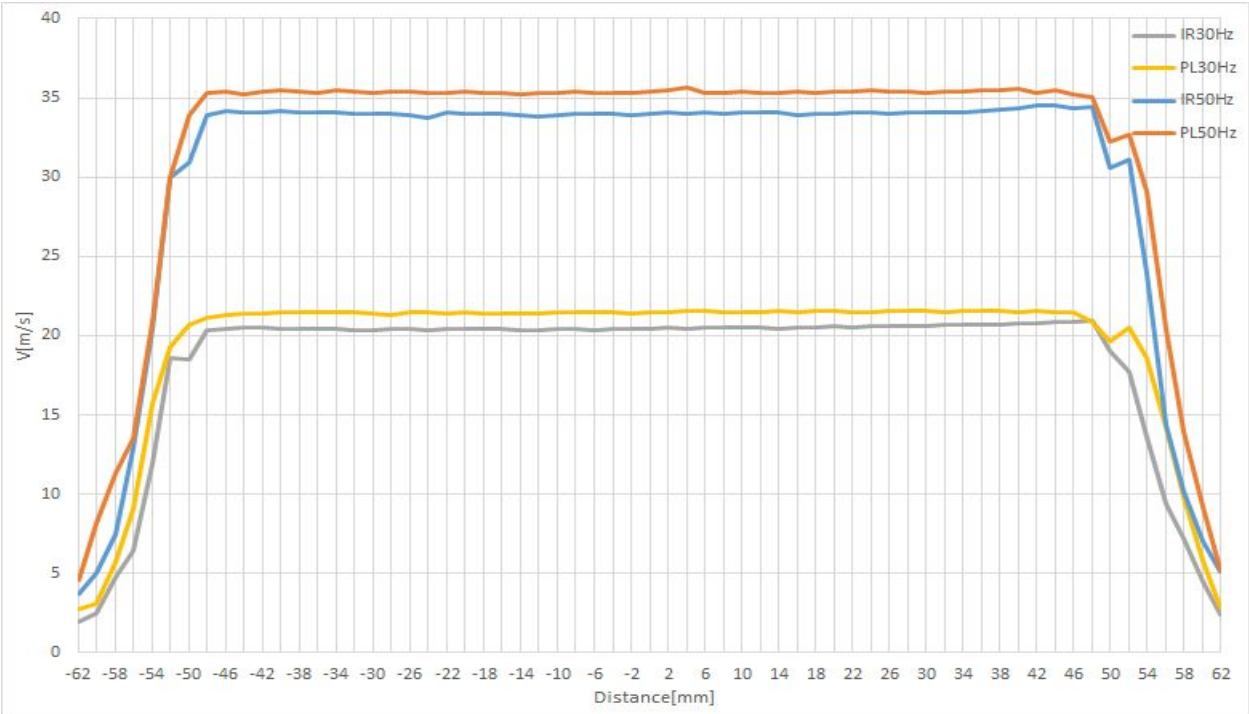

Figure 3-18 Velocity profile for Iron plate and plexiglass plate with diameter 11 mm and different frequencies of the fan.

It was to be expected that with the decrease in the thickness of the plates from 6mm in the case of plexiglass to 1 mm in the case of the iron plate that the velocity would either increase or decrease in an obvious manner. But from the previous graphs, it's easy to see that there is only a slight increase in the velocity of airflow with different diameters and different fan frequencies which also varied between plexiglass and iron. Furthermore, no increase in the static overpressure in the nozzle was recorded on the manometer. There are also some noticeable changes in the shape of the flow field between plexiglass and iron. However, the difference could be more visible with aerodynamic noise measurements.

3.4 Verification of the Measurements

The aim of this subchapter is to confirm that measuring the mean airflow velocity 3 mm above the leaks would result in an accurate representation of the dominant flow field as well as to test whether the free jet flow theory for a nozzle[10] would apply to the leaks.

To verify that, the probe, mounted on the traverse, was set at a height of 3 mm above the leaks and precisely in the middle of the leaks [x=0, z=3]. The traverse was then programmed to move upwards with a 1 mm step until the height of 33 mm was reached. This method was followed for diameter 2,2 mm for both plexiglass and iron plates as it was feared for the probe to get any closer to the leaks and sustain damage by even slightly grazing the surface. For higher diameters(4,4/6,6/8,8 and 11 mm), the probe was set to start 2 mm inside the leaks [x = 0, z = -2] since the leaks were big enough for the probe to measure the flow field inside the leaks without fear of damaging it. The maximum heights set for the traverse to travel upwards were: z = 38 mm for diameter 4,4 mm, z = 48 mm for diameters 6,6 and 8,8 mm, and z = 58 mm for diameter 11 mm. The ventilator fan speed was set only at 50 Hz. The graphs were separated for higher and lower diameters for better representation. The results are as follows:

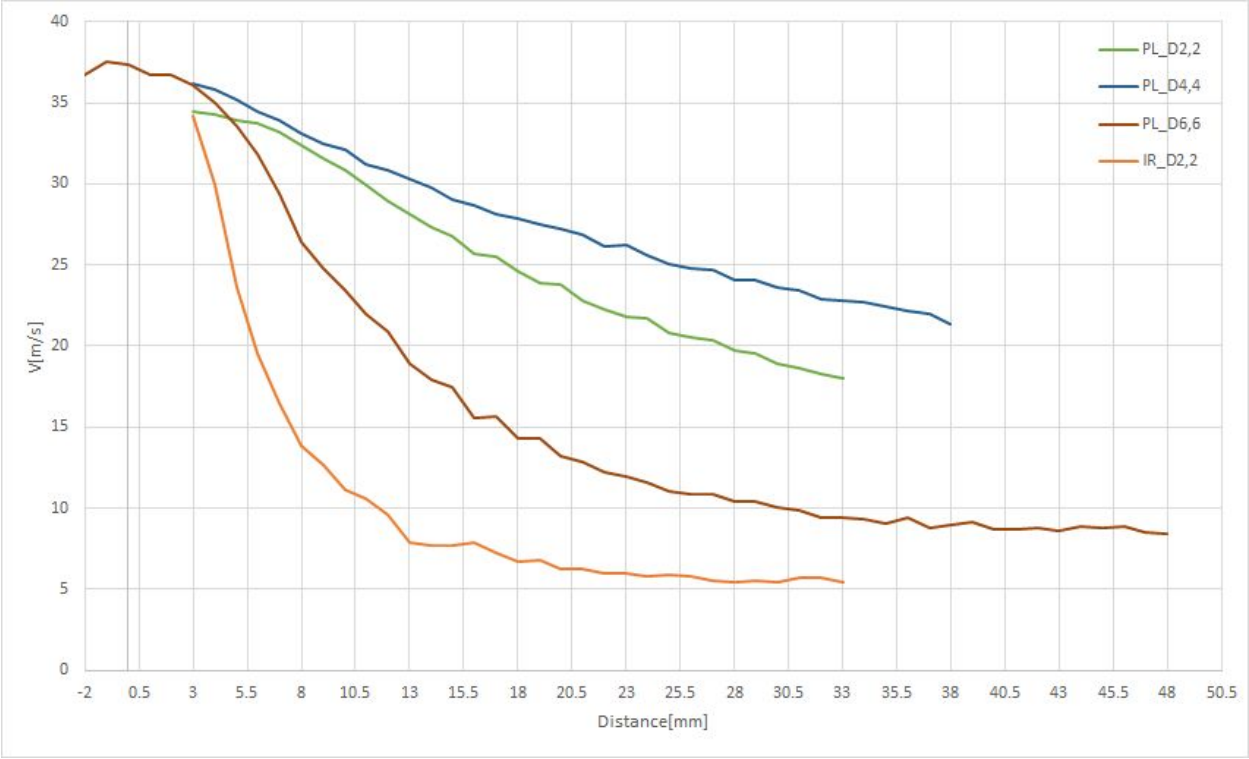

Figure 3-19 Velocity profile above the leaks at 50 Hz for lower diameters

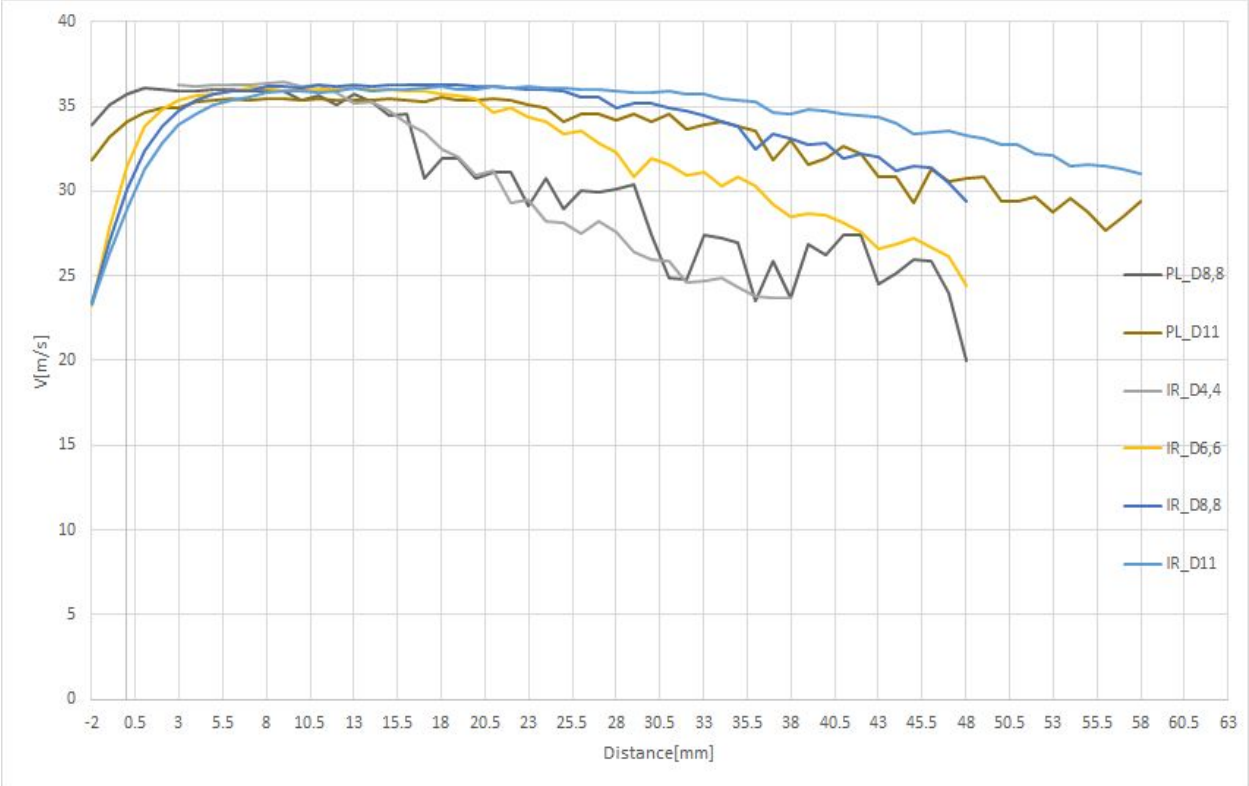

Figure 3-20 Velocity profile above the leaks at 50 Hz for higher diameters

From Figure 3-19, it can be observed that for lower diameters of the leaks, the free jet theory for a nozzle doesn't apply for either iron or plexiglass plates as the flow field enters the turbulent zone as soon as the airflow exits the leaks (i.e, there is no core for such small diameters). With the increase in the diameter as in Figure 3-20, the velocity becomes more uniform inside the potential core (see Figure 3-21) where the flow field has less intensity of the turbulence, until a certain distance(13 mm for diameter 4,4 for iron and diameter 8,8 for plexiglass and 23 mm for diameters 6,6/8,8 and 11 for iron and diameter 11 for plexiglass) from the edge where the flow becomes fully turbulent. For the iron plate, it can be seen that even with smaller diameters of the leaks, the airflow is still inside the core as in diameters 4,4 and 6,6 which is not the case for plexiglass where the flow drops dramatically.

To conclude: For smaller diameters of the leaks, the theory of the free jet flow core doesn't apply, but applies for higher diameters. With the increase in the thickness of the plate, as in the case for plastic plate, the core becomes shorter due to the increased influence of the edge of the plate. And with the decrease in thickness, the impact of the edge of the plate on the airflow is reduced. Nonetheless, this only proves that the measurements done at 3 mm above the leaks, where the airflow is at its peak, are valid for both plexiglass and iron plates at all different diameters of the leaks.

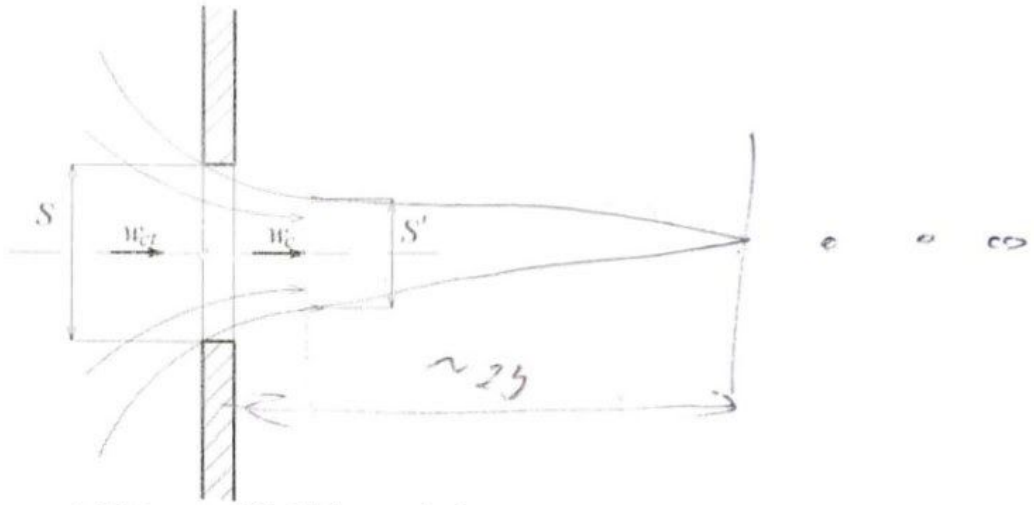

Figure 4. Exhaust of fluid from a hole

Figure 3-21 Exhaust of fluid from a hole[7]

3.5 Tunnel Constant

Before the measurements of the aerodynamic noise could be started, a relation between static and dynamic pressures needed to be evaluated. The tunnel constant equation is necessary for the determination of the static overpressure in the nozzle when the dynamic pressure is known or vice versa. It is determined from the following equation:

$$Xi = \frac{p_d}{\Delta p_s} \tag{1}$$

Where:

Xi	[-]	tunnel constant,
P_d	[Pa]	dynamic pressure,
P_s	[Pa]	static overpressure.

Dynamic pressure is determined from the average velocities of the air 3 mm above the surface of the leaks and the density of air in the room using the following equation:

$$p_d = \frac{1}{2}.\rho.v_s^2 \tag{2}$$

Where:

ρ	[kg/m^3]	density of air,
v_s	[m/s]	average velocity of air 3 mm above the leaks.

And the density of air is calculated using the equation:

$$\rho = \frac{p_b - 0{,}378.p_v}{r_a.(t_d + 273{,}15)} \tag{3}$$

Where:

p_b [Pa] barometric Pressure,

p_v [kg/m^3] saturated vapor pressure,

r_a [J/Kg/K] specific gas constant of dry air,

t_d [°C] dry bulb temperature.

The barometric pressure was measured in the lab using a stationary barometer. Saturated vapor pressure was evaluated from the h-x diagram using dry and wet bulb temperatures, which were measured using an Assman psychrometer.

Static overpressure is induced in the nozzle when the ventilator fan is turned on and it is necessary to allow air to flow through the duct. The static overpressure was measured using a MEDM 500 micromanometer which was connected to the nozzle through a PVC tube which was in turn connected to the nozzle.

The calculations for tunnel constant were done only for the plexiglass, as there was no need to determine the tunnel constant for the iron plate since only two velocities have been measured and the same will be used in the aerodynamic noise measurements.

The following table shows the mean airflow velocity above the plexiglass plate leaks, the tunnel constant, static overpressures, and dynamic pressures for different diameters of the leaks and different frequencies of the fan.

Table 3-1 - Tunnel Constant values for plexiglass plate

Diameter [mm]	Fan Frequency[Hz]	Mean velocity [m/s]	Dynamic Pressure [Pa]	Static Overpressure[Pa]	Tunnel Constant[-]
2,2	10	7,15	32,2	29,65	0,92
	20	11,95	72,77	129,8	0,64
	30	20,57	245,40	293,7	0,84
	40	27,98	453,95	524,4	0,87
	50	34,59	694,02	816	0,85
4,4	10	7,66	34,06	32,7	1,04
	20	15,22	134,29	130,6	1,03
	30	22,45	292,34	294,7	0,99
	40	29,88	517,8	525,5	0,99
	50	35,94	749,29	817,3	0,92
6,6	10	7,4	31,77	32,5	0,98
	20	14,8	127,12	129,9	0,98
	30	21,62	271,14	293,4	0,92
	40	28,13	459,07	524,5	0,88
	50	36,08	755,11	810,3	0,93
8,8	10	7,29	30,78	32,4	0,95
	20	14,46	123,02	129,4	0,95
	30	21,58	277,51	293,1	0,95
	40	28,56	490,33	523,1	0,94
	50	35,25	759,07	808	0,94
11	10	7,15	29,69	32,3	0,92
	20	14,46	121,31	129,5	0,94
	30	21,58	270,12	292,5	0,92
	40	28,56	473,24	522,2	0,91
	50	35,25	720,85	807,7	0,89

4. Measuring Aerodynamic Noise

Now that the airflow velocities over the leaks have been evaluated, and a relation between the dynamic pressures and static overpressures in the nozzle has been created, the stage is set to measure the aerodynamic noise generated by the leaks.

The aerodynamic noise measurements were done in the same acoustics lab as the airflow measurements. However, the measurements had to be done after midnight to ensure that the background noise is at a minimum level.

Five microphones were used to measure the sound pressure level at 5 points around the leaks. Two microphones were set parallel to the leak ends, and two microphones perpendicular to it all opposite to each other. The fifth microphone was set between two of them as will be shown in Figure 4-1. The microphones were set at a distance of 1 meter for the edge of the nozzle and 1.83 meters from the ground level at a 45° angle to guarantee the measurement of the direct sound waves out of the leaks.

The aim of this measurement is to evaluate the aerodynamic noise generated by the leaks across different diameters. Aerodynamic noise generated is presented as a sound power level, which can be calculated from the average sound pressure levels registered by each microphone. A relation between generated sound power level and the frequency at each third-octave band was then generated, as well as the relation between Strouhal number and relative sound power levels for each diameter of the leaks.

Sound power level is calculated using the equation:

$$L_w = L_p + 10 \cdot Log(S) \quad (4)$$

Where:

L_w [dB] sound power level,

L_p [dB] sound pressure level,

S [m^2] area of half sphere.

The logarithmic average of the sound pressure levels over the third-octave bands recorded by each microphone was determined from the equation:

$$L'_p = 10 \,.\, log(\tfrac{1}{N} \,.\, \sum_{i=1}^{N} 10^{\,0,1 \,.\, L_i}) \tag{5}$$

Where:

L'_p [dB] average sound pressure level,

N [-] number of measuring points,

L_i [dB] sound pressure level.

The sound pressure level needs to be corrected for the background noise levels using the following equation:

$$L_p = 10 \,.\, log(10^{\,0,1 \,.\, L_p} - 10^{\,0,1 \,.\, L_{p,background}}) \tag{6}$$

Where:

L_p [dB] corrected sound pressure level,

L_p [dB] sound pressure level for a given third-octave band,

$L_{p,background}$ [dB] background noise level for a given third-octave band.

However, background noise levels couldn't be corrected for lower frequencies of the fan at 10 Hz and 10 m/s(determined by the tunnel constant) as the corrected sound pressure level was found to be negative and zero in some cases. The following table shows the corrected sound pressure level for 10 Hz and 10 m/s across some diameters of the leaks.

Table 4-1 - Corrected background noise levels

f[Hz]	$L_{p,10HzD2,2}$ [dB]	$L_{p,10msD2,2}$ [dB]	$L_{p,10HzD4,4}$ [dB]	$L_{p,10msD4,4}$ [dB]	f[Hz]	$L_{p,10HzD2,2}$ [dB]	$L_{p,10msD2,2}$ [dB]	$L_{p,10HzD4,4}$ [dB]	$L_{p,10msD4,4}$ [dB
20	9,2	5,3	Error	Error	630	-19,5	13	30,6	16,6
25	21,5	29,2	21,8	23,8	800	-21,4	17,3	30,4	37,2
31.5	21,2	27,3	21,6	22,1	1000	Error	23,3	7,2	31,8
40	11,9	12	5,6	4,2	1250	-9,2	18,6	12,3	12,4
50	Error	14,7	18,3	1	1600	-5,1	27,7	7,1	17,6
63	-1,5	14,4	12,6	10,6	2000	-24,2	39	-6,1	5,1
80	-2	12,8	-1,6	5,2	2500	Error	13,8	15,1	-1,1
100	-1,4	11,2	0,4	5,9	3150	Error	14,2	Error	-9,6
125	4,6	1,3	1,8	9,5	4000	Error	15,8	Error	-17,5
160	-0,9	3,4	2,1	10,6	5000	Error	2	Error	Error
200	-7,3	3	-2,2	8,7	6300	Error	-2,3	Error	-18,2
250	-7,9	7,3	-2,1	13,3	8000	-19,9	-8,3	-16,4	-14,5
315	Error	9	23,3	14,4	10000	Error	-16,6	Error	-18,2
400	-11,7	17,1	17,4	25,5	12500	Error	Error	Error	Error
500	Error	15,8	7,9	20,7	16000	-5	-12,7	-5	-4,4

From Table 4-1, negative values arise when the logarithm function in equation (6) is less than 1, and errors arise when the background noise levels are higher than the average sound pressure levels recorded by microphone. Different values, but the same results were calculated for different diameters at 10 Hz and 10 m/s. For this reason, the following data presented will be without correction of the background noise to maintain systematic results.

The aerodynamic noise measurements were done for some standard frequencies of the ventilator fan(10, 30, and 50 Hz) for plexiglass plate and only 30 and 50 Hz for the iron plate, and some desired mean airflow velocities(10, 15, and 25 m/s) only for plexiglass plate. The equivalent of fan frequency to the mean airflow velocity measured in chapter (3) which will be extensively used in this chapter is shown in the following table:

Table 4-2 - Values of Mean airflow velocity with respect to fan frequency

Diameter[mm]	Fan Frequency[Hz]	Mean velocity (PL) [m/s]	Mean velocity (IR) [m/s]
2,2	10	7,15	-
	20	11,95	-
	30	20,57	22,20
	40	27,98	-
	50	34,59	35,37
4,4	10	7,66	-
	20	15,22	-
	30	22,45	22,10
	40	29,88	-
	50	35,94	36,38
6,6	10	7,4	-
	20	14,8	-
	30	21,62	21,61
	40	28,13	-
	50	36,08	35,55
8,8	10	7,29	-
	20	14,46	-
	30	21,58	21,05
	40	28,56	-
	50	35,25	35
11	10	7,15	-
	20	14,46	-
	30	21,58	20,55
	40	28,56	-
	50	35,25	34,17

4.1 Measurement procedure:

1- First, the microphones were fixed around the nozzle in a manner that ensures the measurements of all the dominant sound field as shown in the following figure:

Figure 4-1 Setup of the aerodynamic noise measurements.

2- The ventilator fan was then turned on, with frequency 10 Hz and the sound pressure levels were registered by the microphones.

3- Then, to achieve the desired 10 m/s velocity, the tunnel constant presented in chapter (3.2) had to be used. By substituting in equations (2) and (1), the static overpressure in the nozzle could be calculated. Then the ventilator fan was manipulated accordingly until the calculated static overpressure was read on the manometer. The same procedure was followed when measuring velocities 15 and 25 m/s.

4- The Frequency of the fan was then set to 30, and 50 Hz respectively.

4.2 Measurements Results

Following results for sound power levels uncorrected by the background noise over the sound spectrum for leaks with diameter 2,2 mm are in Figure 4-2:

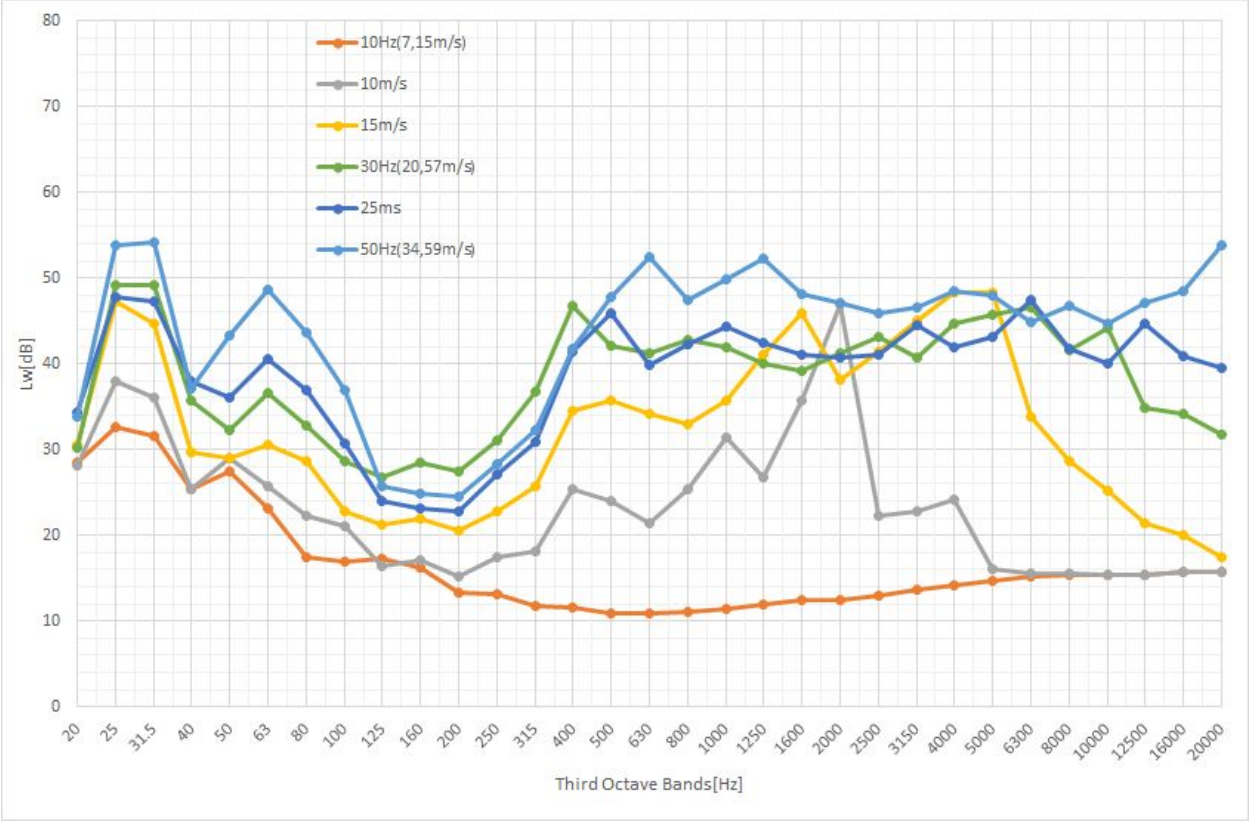

Figure 4-2 Spectrum of Sound Power level for diameter 2,2 mm across all velocities

6- The diameters of the leaks were increased to 4,4/6,6/8,8 and 11 mm respectively while following the same procedure as for diameter 2,2. The graphs are presented as follows:

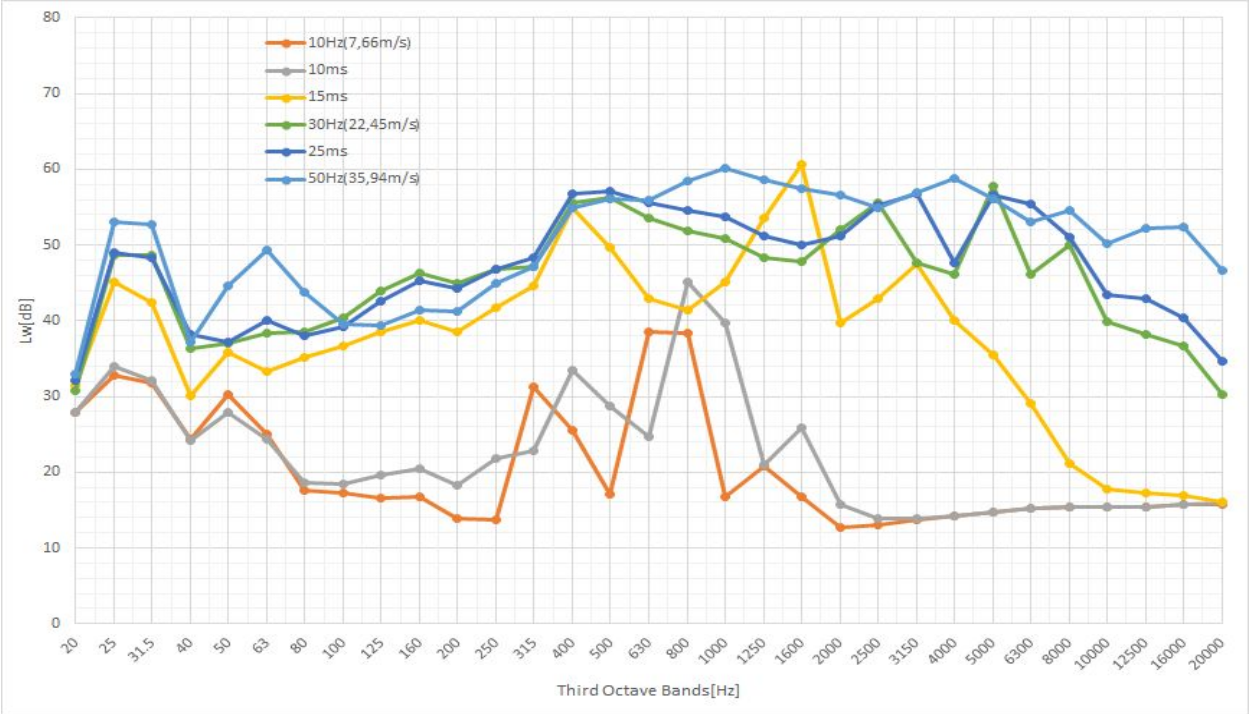

Figure 4-3 Spectrum of Sound Power level for diameter 4,4 mm across all velocities

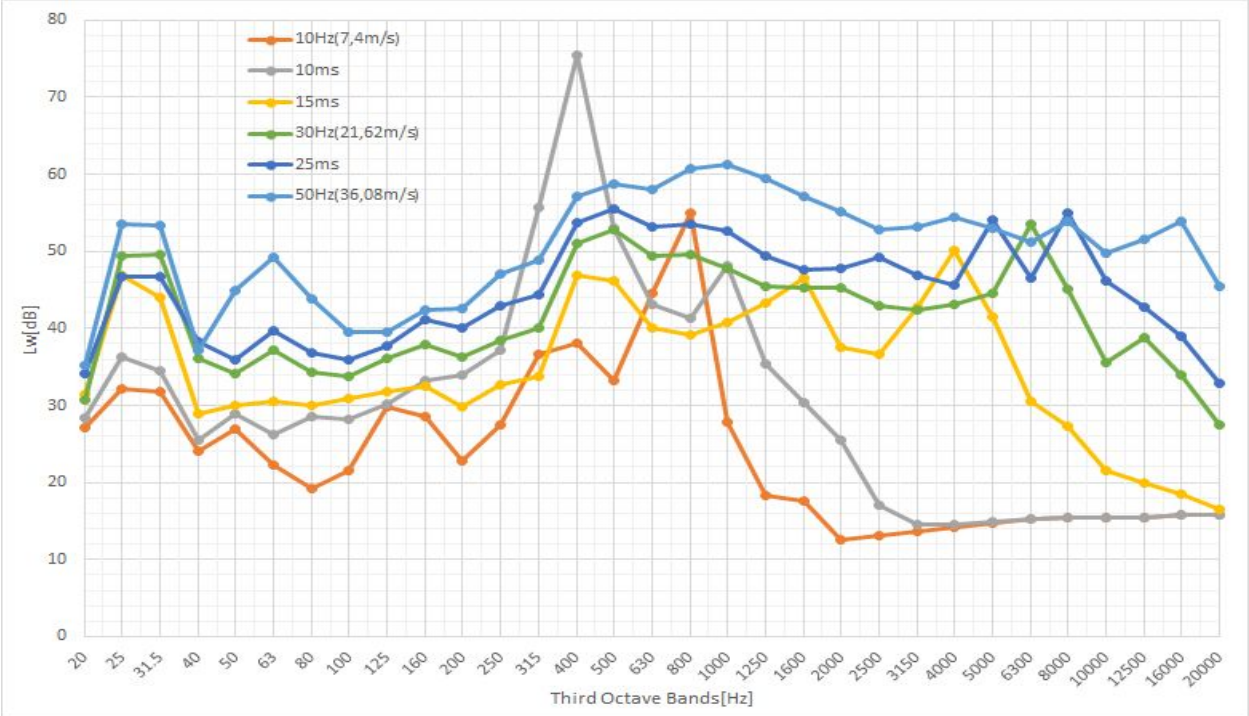

Figure 4-4 Spectrum of Sound Power level for diameter 6,6 mm across all velocities

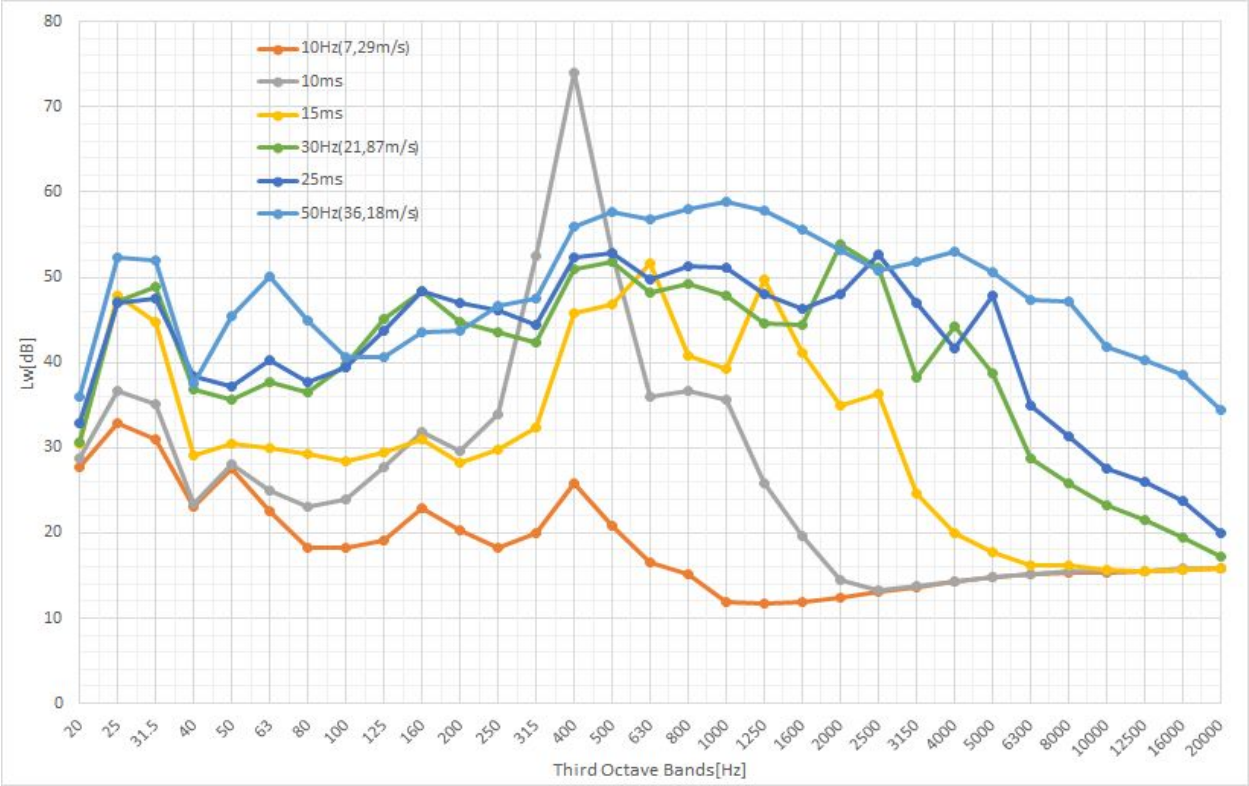

Figure 4-5 Spectrum of Sound Power level for diameter 8,8 mm across all velocities

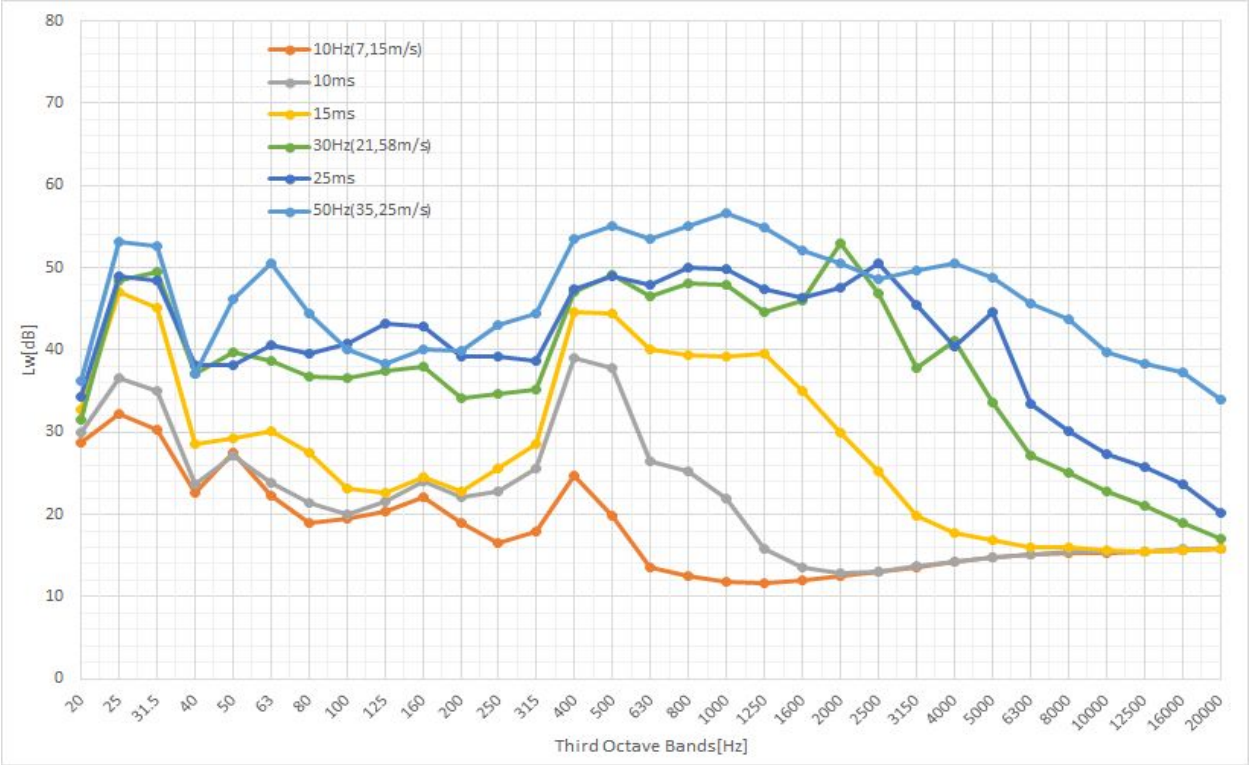

Figure 4-6 Spectrum of Sound Power level for diameter 11 mm across all velocities

From the previous figures, at lower frequencies(between 20 and 40 Hz) a peak in the acoustic spectrum can be seen across all diameters and velocities. This is caused by the ventilator fan which wasn't built to withstand the high static overpressure in the duct system caused by the leaks. But this shouldn't have an impact on the aerodynamic noise measurements though since the influence of the leaks is dominant at higher frequencies. It can be seen that for higher velocities(30Hz, 25m/s, and 50 Hz) for any given diameter of the leaks that the aerodynamic noise over the sound spectrum is somewhat uniform, i.e, the aerodynamic noise doesn't have any tonal component that can be seen in lower velocities. For lower velocities(10Hz, 10, and 15m/s) tonal components can be seen, some more clearly than others, as is the case with velocity 10 m/s at diameter 6,6 and 8,8 mm at frequency 450Hz and sound power level 76 and 74 dB, velocity 10 Hz for diameter 6,6 mm at 800 Hz and 55 dB, 15 m/s for diameter 4,4 mm at 1600 Hz and 61 dB, and 10 m/s for diameter 2,2 mm at 2000 Hz and 47 dB. There was no vibration whatsoever associated with the aerodynamic noise generated by those tonal components, only shear aerodynamic noise.

This can be explained by the presence of intensive vortices that occur at the edge of the leaks. Higher velocity of air through the leaks is associated with higher turbulence, with higher turbulence, the tonal components created by the vortices are masked. At lower velocities, the tonal components become dominant because the turbulence is less chaotic and the other tonal components are dampened. Aerodynamic noise can be imagined by imagining every vortex as a sound source, and with the presence of many loud and chaotic sound sources, it's more difficult to distinguish a specific one. While with lower velocities/less turbulence, a specific tonal component that is intensive enough, is distinguishable. When the tonal components are not the prevalent source of noise, it can be seen that with the increase in airflow velocity, the aerodynamic noise naturally increases due to the increase in turbulence.

Another form of displaying the tonal components can be shown when comparing the same velocity over different diameters as shown in the following graphs:

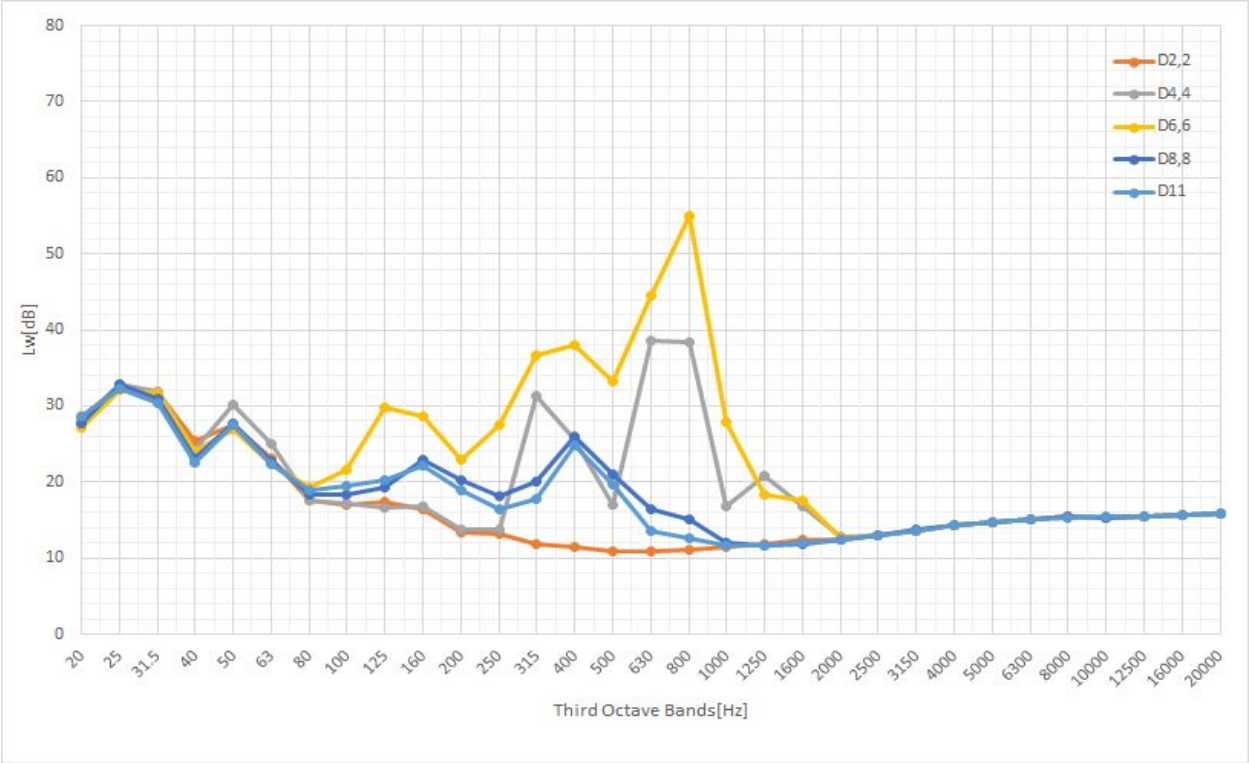

Figure 4-7 Spectrum of Sound Power level for velocity 10 Hz across all diameters

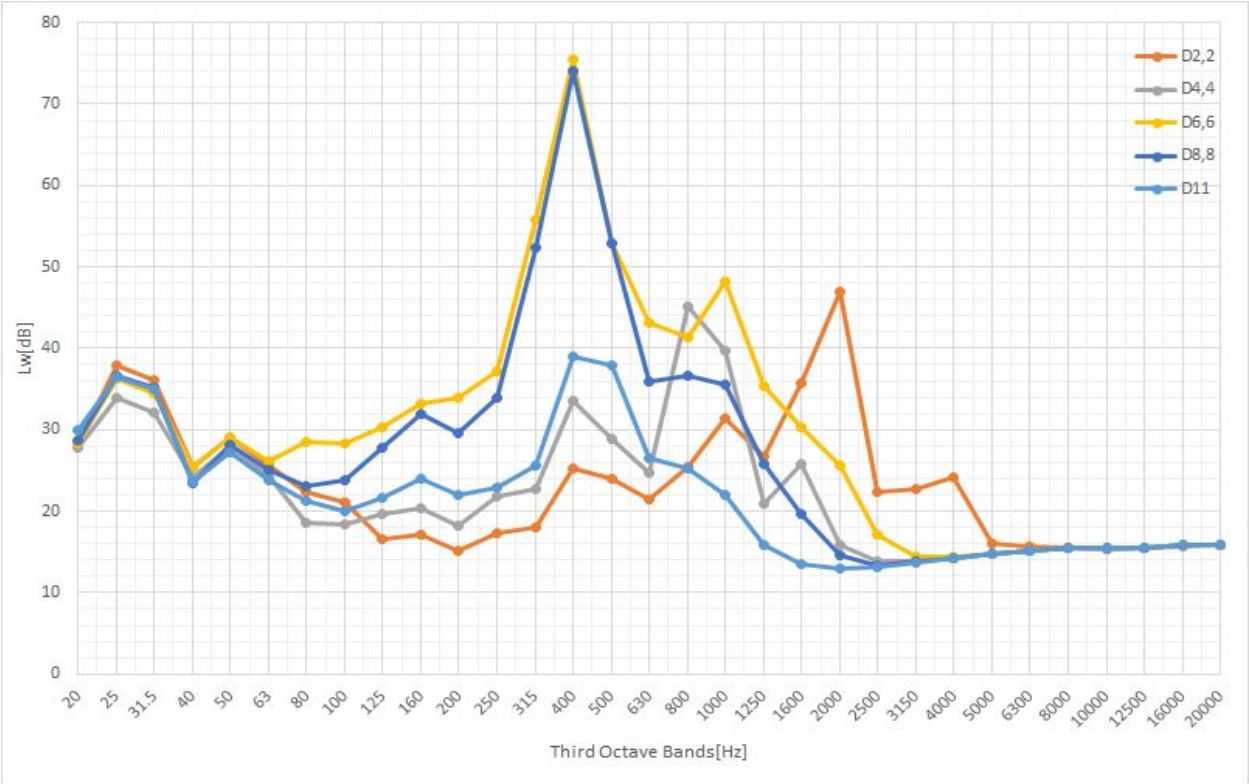

Figure 4-8 Spectrum of Sound Power level for velocity 10 m/s across all diameters

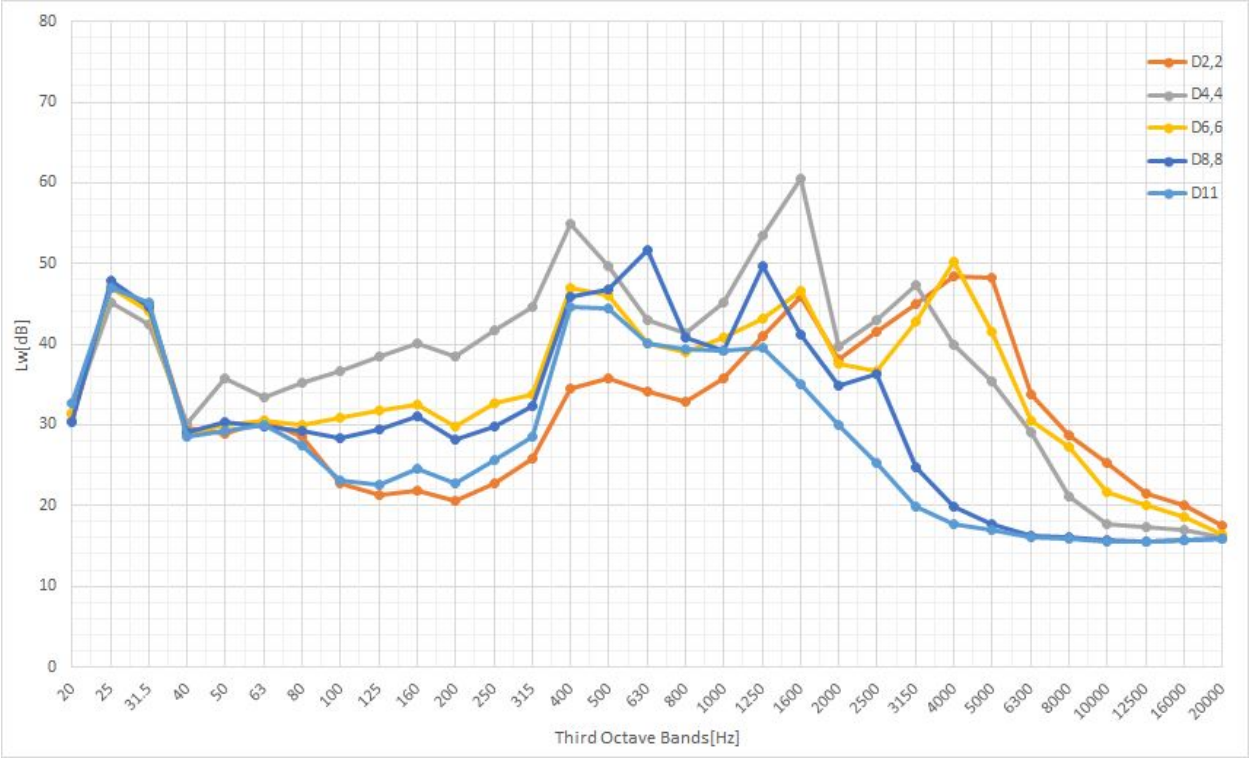

Figure 4-9 Spectrum of Sound Power level for velocity 15 m/s across all diameters

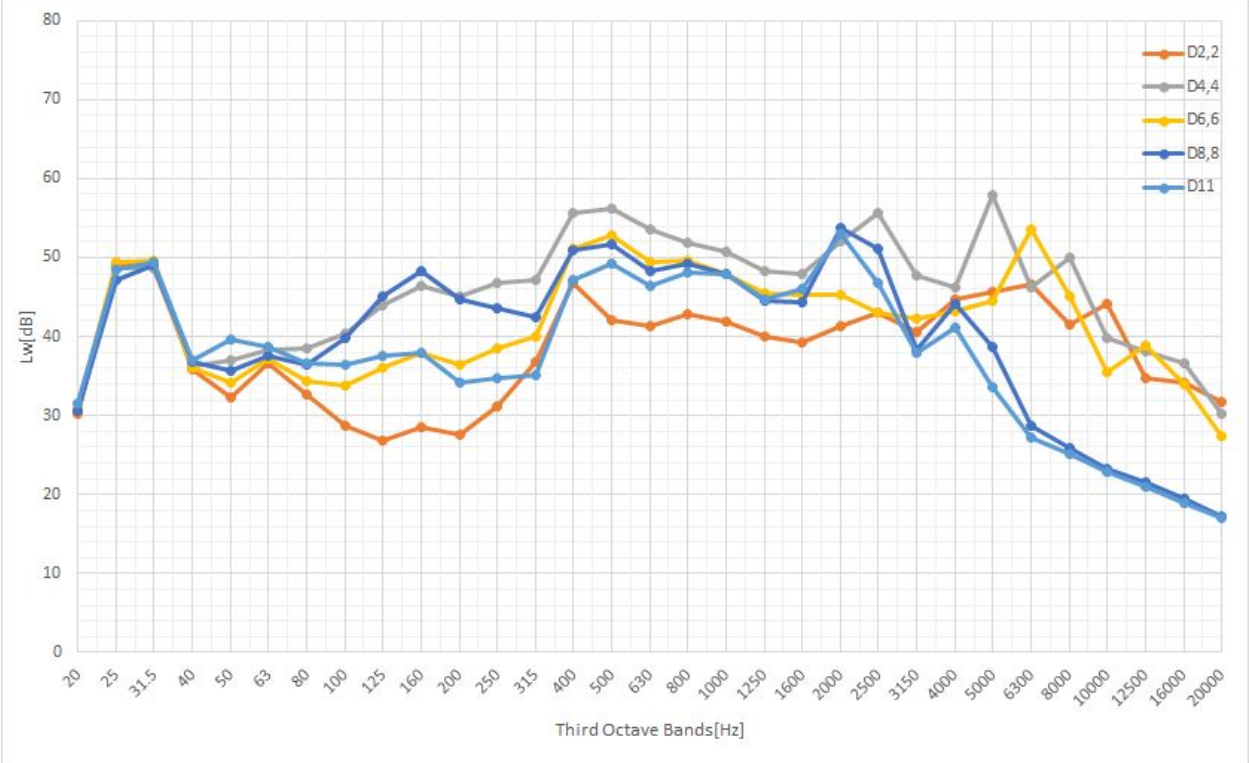

Figure 4-10 Spectrum of Sound Power level for velocity 30 Hz across all diameters

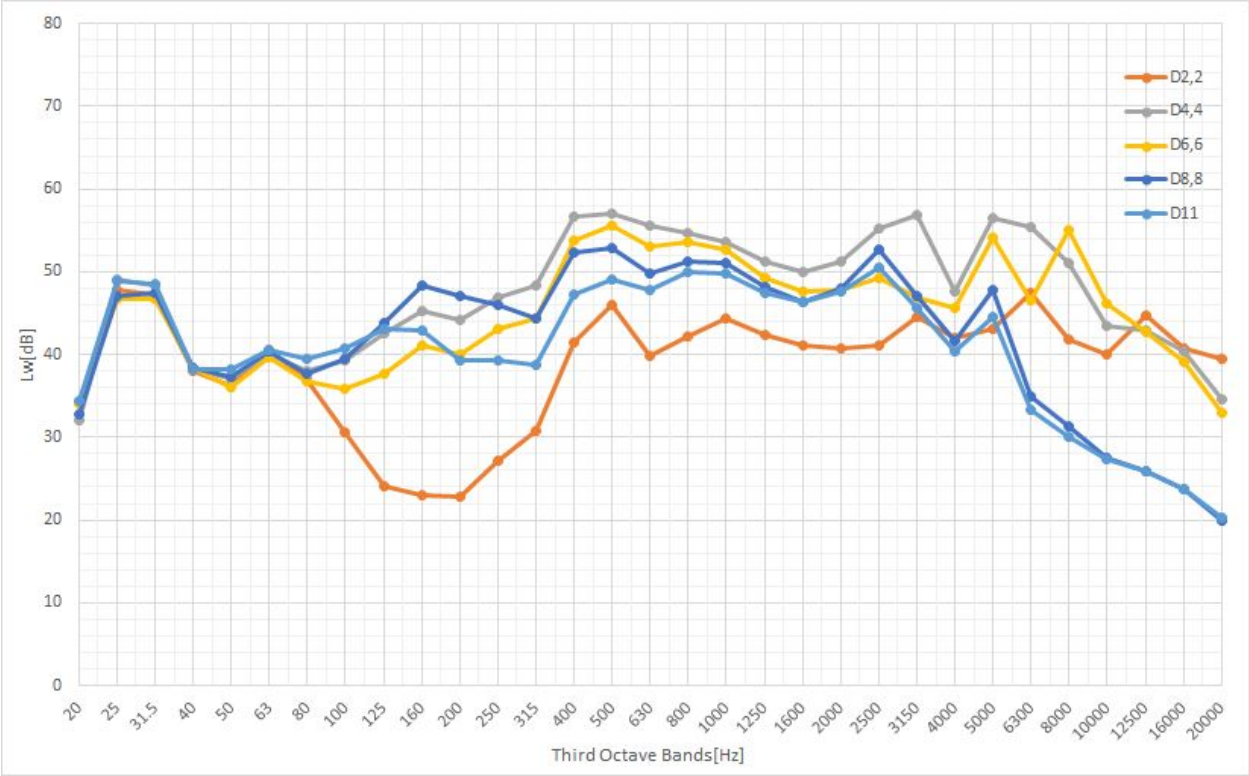

Figure 4-11 Spectrum of Sound Power level for velocity 25 m/s across all diameters

Figure 4-12 Spectrum of Sound Power level for velocity 50 Hz across all diameters

As shown in the graphs above, the intensive tonal components are at their peak at velocity 10 m/s and diameters 6,6 and 8,8 mm, some can be found also for velocity 10 Hz and 15 m/s, while they almost disappear for higher velocities. Previous graphs also show that diameters 4,4 and 6,6 mm emit the most overall aerodynamic noise across the spectrum at various fan velocities.

After measuring the aerodynamic noise caused by plexiglass leaks, the iron plate was used again as in chapter (3). Once again, the aim is to see whether the change of plate diameter from 6mm to 1mm would cause an increase or decrease in the aerodynamic noise caused by the leaks. The measurements were done for ventilator fan speed at 30 Hz and 50Hz whose equivalent mean velocities can be found in Table 4-2. I will present the results of the iron plate as a comparison with the plexiglass plate. The comparison will be done over two graphs, one is showing all the diameters of the leaks for both plexiglass and iron plate for frequency 30Hz, and the other for frequency 50Hz. The results are as follows:

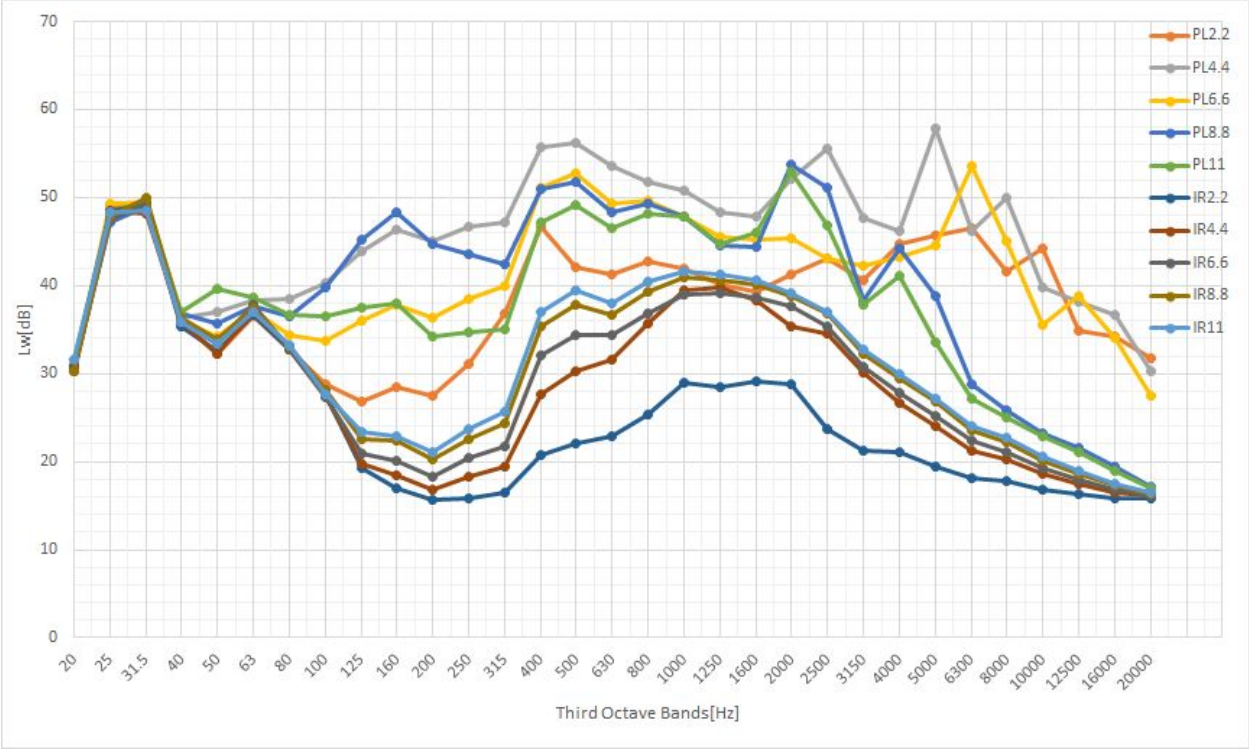

Figure 4-13 Spectrum of Sound Power level for Iron plate and plexiglass plate at 30Hz across all diameters

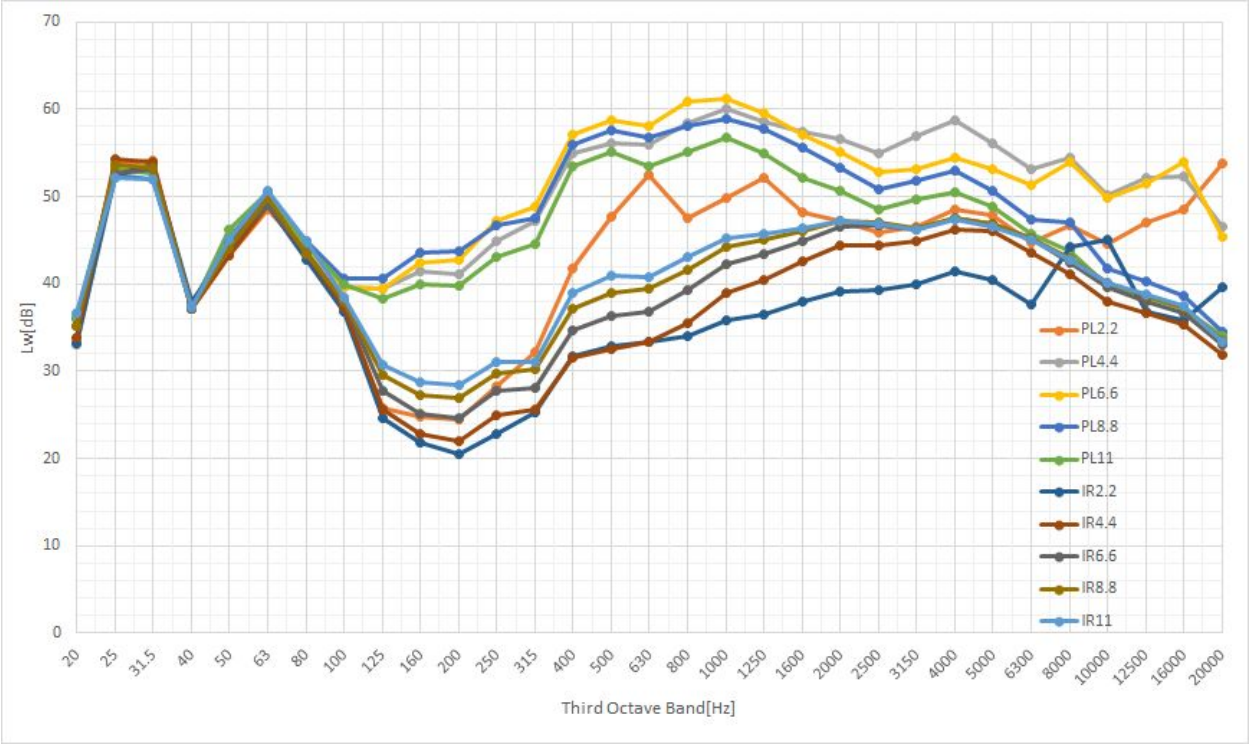

Figure 4-14 Spectrum of Sound Power level for Iron plate and plexiglass plate at 50Hz across all diameters

From the previous figures, the aerodynamic noise created by the plexiglass leaks is shown to be louder than that of the iron plate for the same fan velocities. Thus, showing that bigger thickness of the plate associates with higher aerodynamic noise. Some small tonal components can be seen for the plexiglass at velocity 30Hz across different diameters and different frequencies, but none can be seen at all for the iron plate.

It is common practice in aerodynamic noise measurements and evaluations to calculate the Strouhal number and relative sound power levels in order to compare the shape of the sound spectra[6]. This will only be shown for the plexiglass plate at some significant velocities. Strouhal number is calculated using the following equation:

$$S = \frac{f \cdot d}{v_s} \tag{7}$$

Where:

S	[-]	Strouhal number,
f	[Hz]	third-octave band frequency,
d	[m]	diameter of the leaks,
v_s	[m/s]	mean airflow velocity 3 mm above the leaks surface.

While relative sound power level is calculated as:

$$L_{w,rel} = L_w - L_{wi} \tag{8}$$

Where:

$L_{w,rel}$	[dB]	relative sound power level,
L_w	[dB]	total sound power level,
$L_{w,i}$	[dB]	spectrum of the sound power level.

From previous graphs, the main dominant source of noise was when the velocity of airflow was set at 10 m/s. So in the next graph, I will present the relation between relative sound power level and Strouhal number for this specific velocity to show the influence of the generated noise:

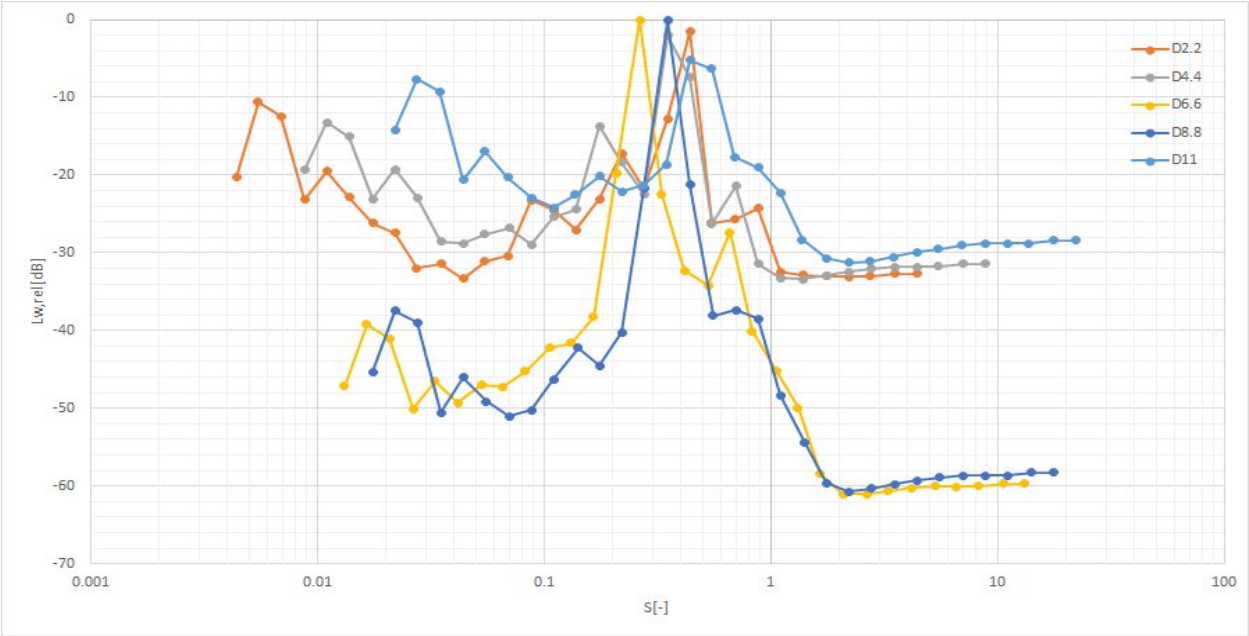

Figure 4-15 Relative sound power level in relation to Strouhal number at 10 m/s

In Figure 4-15, the highest peaks are for diameters 6,6 and 8,8 mm with Strouhal peaks at S = 0,26 and 0,35. Lower peaks can be found for diameter 2,2 mm at S = 0,44 and for diameter 4,4 mm at S = 0,35. This shows how the aerodynamic noise generated by this specific velocity is influenced by diameters 2,2/4,4/6,6 and 8,8 mm almost to the same degree.

Another significant Strouhal peak at 0,71 can be found for velocity 10 Hz and diameter 6,6 mm as shown in the following figure:

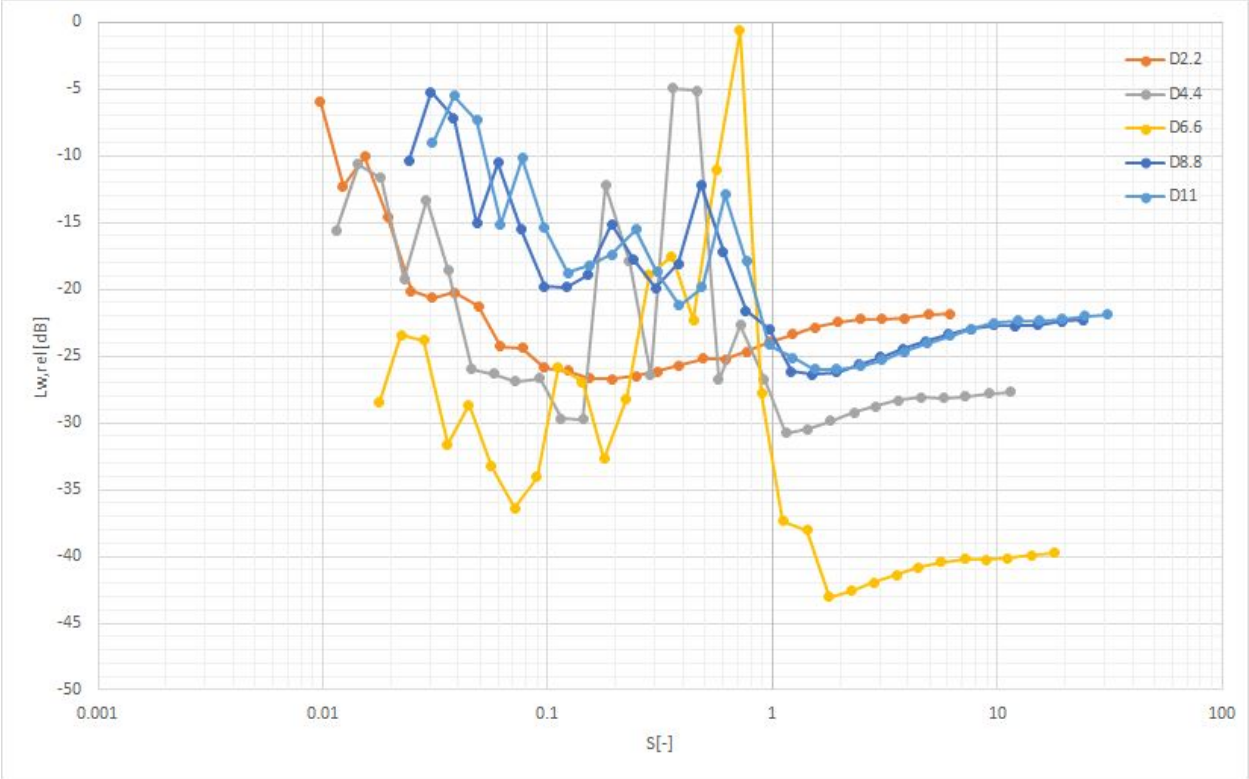

Figure 4-16 Relative sound power level in relation to Strouhal number at 10 Hz.

When comparing relative sound power level in relation to Strouhal number for the same diameter across different velocities, more peaks were found. The most significant ones were found at diameters 4,4 and 6,6 mm and will be shown in the next couple of graphs.

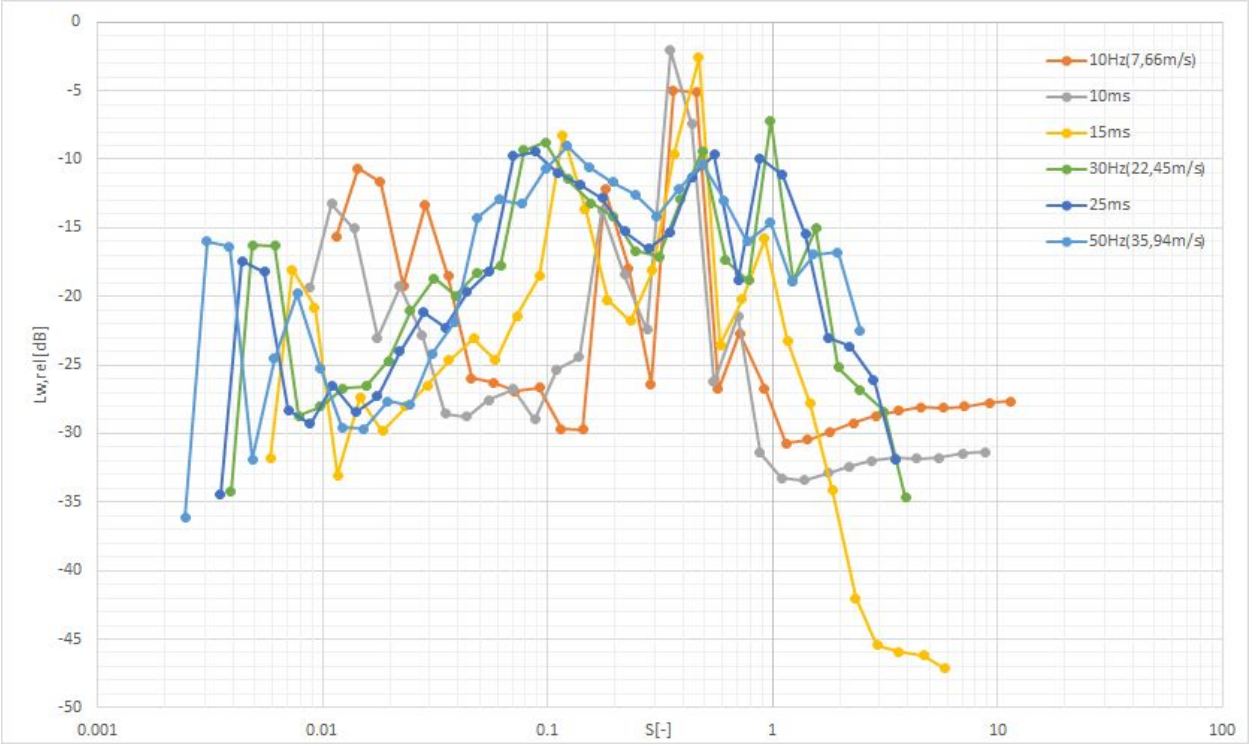

Figure 4-17 Relative sound power level in relation to Strouhal number for diameter 4,4 mm

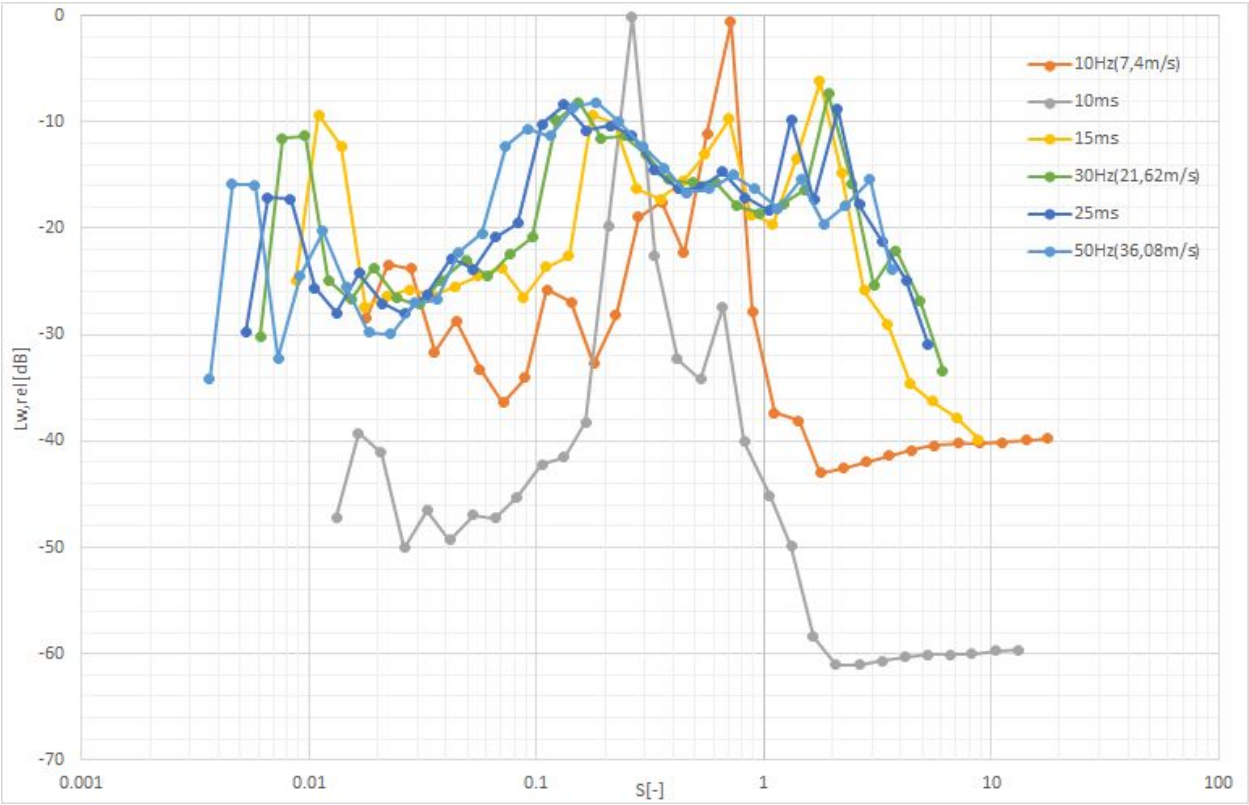

Figure 4-18 Relative sound power level in relation to Strouhal number for diameter 6,6 mm

The importance of Strouhal number comparison to relative sound power level can be seen in the previous graphs. While Figures 4-3 and 4-4 show the decibel values of the aerodynamic noise, they don't show which velocities influence the noise the most as in Figures 4-17 and 4-18 that show that for diameter 4,4, velocities 10 and 15 m/s have almost the same influence on the noise with Strouhal peaks at 0,35 and 0,45 respectively. Velocity 10 Hz also has some influence with two lower peaks at 0,36 and 0,46. For diameter 6,6 mm, Strouhal peaks are also observed for velocities 10 Hz and 10 m/s at S = 0,26 and 0,71 respectively.

No significant Strouhal peaks were found in the relative sound power level spectra for other velocities or diameters. For the iron plate, no significant Strouhal peaks were found for the 30 Hz or 50 Hz frequencies.

Another typical calculation for the aerodynamic noise is the relation between total sound power levels[6] corrected and uncorrected by filter A to the logarithm of the mean airflow velocity 3mm above the leaks for plexiglass plate. Filter A is a measurement of the sound power or pressure levels with corrections to the sensitivity(perception) of the human ear. And can be calculated as:

$$L_{wA} = 10 \,.\, log(\sum_{i}^{n} 10^{\,0,1(L_{wi}+K_{Ai})} \tag{9}$$

Where:

L_{wA} [dB] sound power level corrected by filter A,

L_{wi} [dB] spectrum of sound power level,

K_{Ai} [dB] weighted filter A.

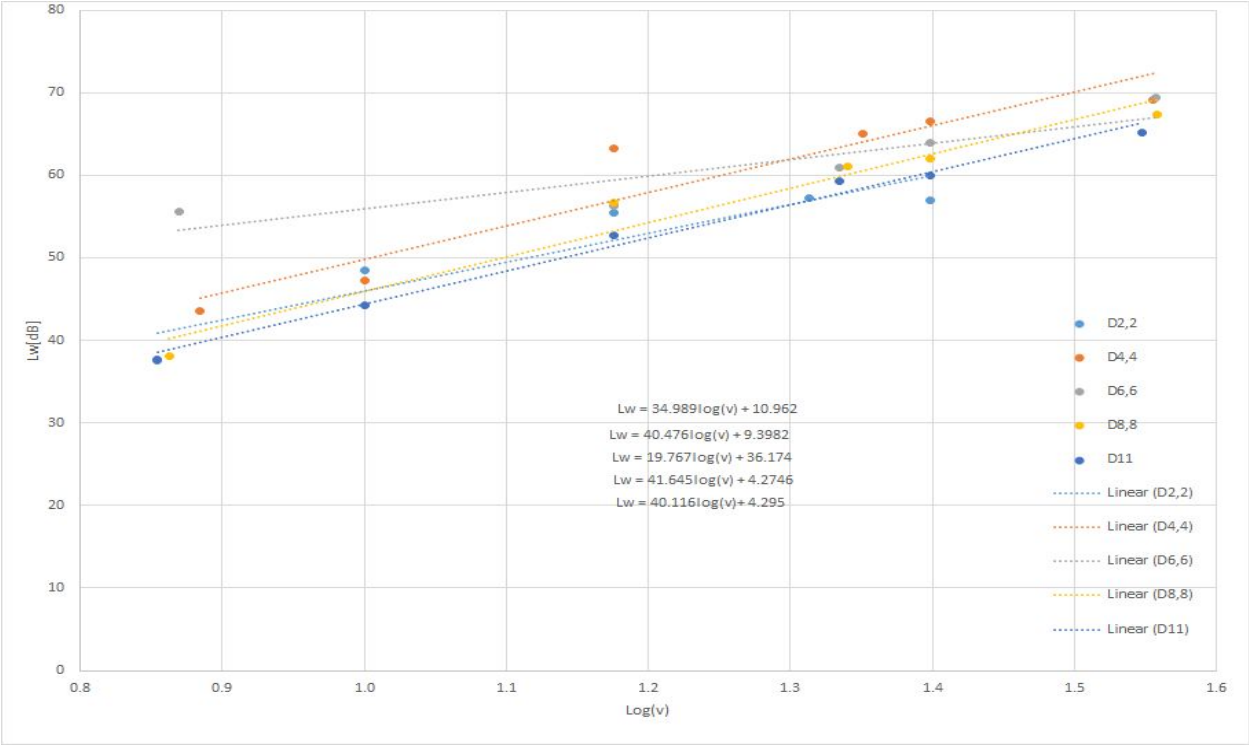

Figure 4-19 Total sound power level in relation to the logarithm of velocity

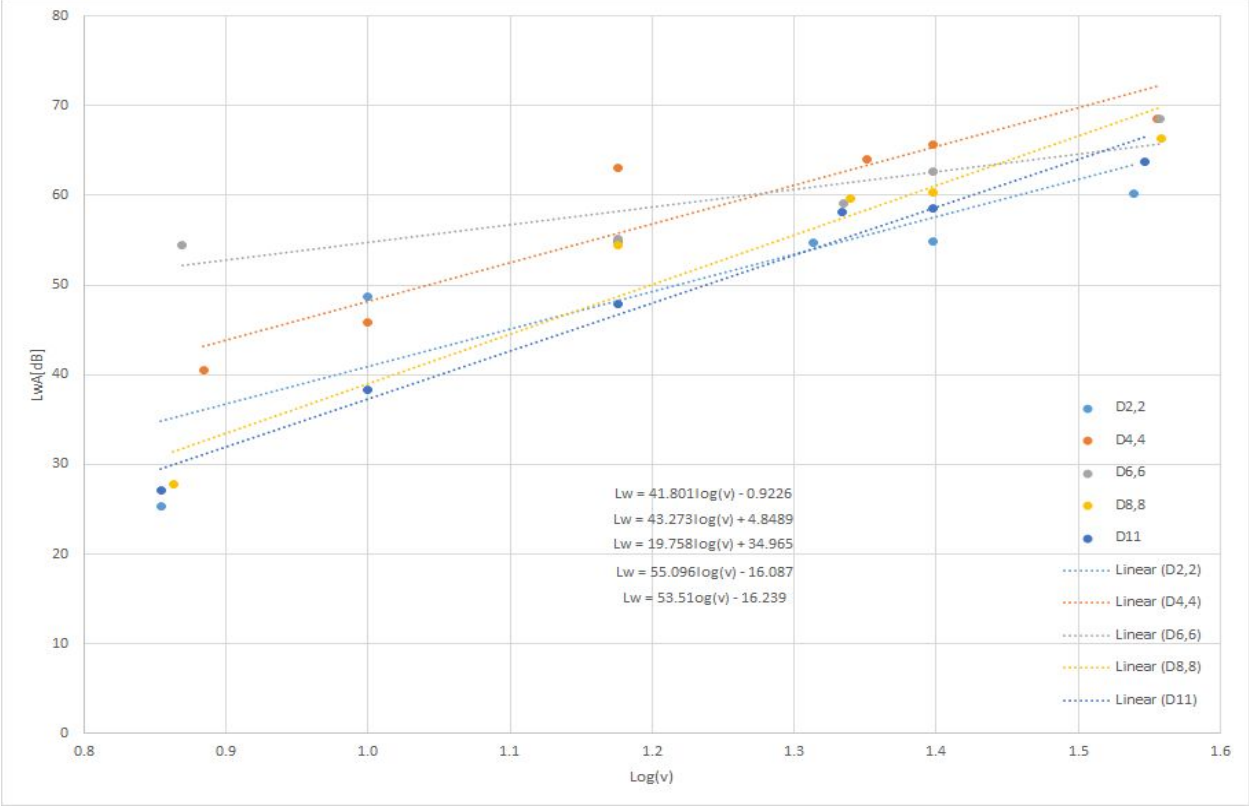

Figure 4-20 Total sound power level corrected by filter A in relation to the logarithm of velocity

Solving the logarithmic relations shown in Figures 4-19, the linear dependence of the logarithm of airflow velocity to the total sound power level is within the range of exponent 2 - 4,2 of the velocity. And from figure 4-20, the linear dependence of the logarithm of the airflow velocity to the total sound power level corrected by filter A is within the range of exponent 2 - 5,5 of the velocity. For the regression lines in the previous diagrams, the logarithm of velocity 10 m/s for diameters 6,6 and 8,8 mm were not taken into account due to their abnormal behavior which doesn't correspond to the linear dependence of the airflow velocity.

5. Conclusion

Through the course of this experimental thesis, the mean airflow velocity over the leaks and the aerodynamic noise caused by it were studied to some extent. The use of two different plates to constrict the airflow over the nozzle was necessary to determine the behavior of the flow field. It was established that for the measurement done 3 mm above the edge of the leaks, both plates had almost the same behavior except for some irregularities as shown in Figures 3-9 and 3-14. Differences arise when measuring the flow field in the direction of increasing turbulence as illustrated in Figures 3-19 and 3-20 where it was evident that for smaller diameters of the leaks the airflow is non-uniform, while for bigger diameters, the flow field becomes more stable and follows the known theory of free jet flow. The influence of the smaller thickness of the plates was also demonstrated to have similar behavior as for the free jet flow theory, unlike bigger thickness.

Aerodynamic noise measurements proved to be quite interesting. The ventilator fan, which wasn't built to withstand such high static overpressures caused by the leaks, proved to be quite problematic. For future measurements of aerodynamic noise, it is advisable to use a ducted system that could withstand such high static overpressure without causing noise at lower frequencies. Background noise levels couldn't be corrected for lower airflow velocities, hence,

all sound power level evaluations were made without background noise correction to maintain uniform results.

Some discreet tonal components were observed for low mean airflow velocities, most noteworthy is 10 m/s, across different diameters of the leaks. For future measurements, it's advisable to make a frequency analysis FFT for the fluctuation of the turbulent flow for those tonal components to better understand their behavior. The comparison of the plexiglass and iron plates for 30 Hz and 50Hz across different diameters resulted in the conclusion that the plexiglass was noisier across all velocities and diameters. It's also advisable to measure the lower velocities for the iron plate for future measurements to check the behavior of the tonal components.

Strouhal peaks were found for velocity 10 m/s across diameters 6,6 and 8,8 mm at S = 0,26 and 0,35, and S=0,71 for velocity 10 Hz at diameter 6,6 mm. Strouhal peaks were also shown when comparing different velocities at the same diameter as in Figures 4-17 and 4-18 and the importance of using such a comparison in aerodynamic noise measurements. Lastly, the linear dependence of the total sound power level to the logarithm of airflow velocity was calculated to be in the exponential range 2 - 4,2 of the velocity and 2 - 5,5 for the total sound power level corrected by filter A.

A considerable amount of data was collected in the preparation of this thesis and most of it couldn't be presented in this file. A CD containing all the calculated data and graphs will be submitted with the printed form.

List of References

[1] Crocker, M. J. (2007). *Handbook of noise and vibration control*. John Wiley.

[2] Barron, R. F. (2003). *Industrial noise control and acoustics*. Dekker.

[3] Glegg, S. A., & Devenport, W. J. (2017). *Aeroacoustics of low Mach number flows: Fundamentals, analysis, and measurement*. Academic Press.

[4] Mak, C., Waddington, D., & Oldham, D. (1997). The Prediction of Airflow Generated Noise in Ventilation Systems. *Building Acoustics, 4*(4), 275-294. doi:10.1177/1351010x9700400404

[5] Long, M. (2014). *Architectural acoustics*. Academic Press.

[6] Kučera, M., Králíček, J.: Aerodynamic Noise of Blade Grill HVAC Systems at Low Mach Numbers. In: 24th International Congress on Sound and Vibration. London, 2017.

[7] Kučera, M., Nový, R.: Noise Generated by Air Flowing From Small Holes. In: Proceedings of the Seventeenth International Congress on Sound and Vibration. Cairo: The International Institute of Acoustics and Vibration, 2010.

[8] Šimunsky, M.: Characteristics of the Experimental Measuring Line. Bachelor's Thesis. Faculty of Mechanical Engineering, Czech Technical University in Prague. Prague,2018.

[9] Miniature wire probe, straight - 5 pcs. package - Dantec Dynamics: Precision Measurement Systems & Sensors. (n.d.). Retrieved from https://www.dantecdynamics.com/product/miniature-wire-probe-straight-5-pcs-package/

[10]Ball, C., Fellouah, H., & Pollard, A. (2012). The flow field in turbulent round free jets. *Progress in Aerospace Sciences, 50*, 1-26. doi:10.1016/j.paerosci.2011.10.002